NTNU

Norwegian University of
Science and Technology

Experimental design and mathematical simulation of hookload while tripping through bends.

Xiyang Xie

Xiyang Xie

TPG4920 Petroleum Engineering Master Thesis

Experimental design and mathematical simulation of hookload while tripping through bends

Trondheim, August 19th, 2015

NTNU Norwegian University of Science and Technology
Faculty of Engineering Science and Technology
Department of Petroleum Engineering and Applied Geophysics

Prosjektoppgave

NTNU
Det skapende universitet

Preface

This thesis is defined by course TPG4920 – Drilling Engineering Specialization at the Petroleum Engineering and Applied Geophysics Department, Norwegian University of Science and Technology.

During the thesis process, my supervisor, Professor Pål Skalle, and I have always kept in close contact. I really appreciate that Skalle provided me with very constructive suggestions and supports. He also helped me to improve my writing skills. I also appreciate PhD candidate Isak Swahn, and Associate Professor Sigve Hovda, who provided the basic mathematical model for the calculation of the dynamic hookload. In addition, I would like to thank PhD candidate Dapeng Zhao, who taught me many skills in programming. I also would like to thank my ex-girlfriend Yuanhua Li, who encouraged me and made me feel loved in the most of time of these two years. Finally, I would like to thank my parents. They sponsored my study abroad and encouraged me at every moment when I feel down and homesick.

Xiyang Xie

Trondheim, August 2015.

Abstract

To meet the growing demand of energy consumption, oil companies are trying their best to produce oil. However, in the past few years, the oil price has kept going down and dampened the whole industry. On one side, oil companies need to satisfy the requirement from the market, on the other hand, they have to keep proper focus on their own growth. Drilling operations, especially offshore are costly. Reducing non-productive time (NPT) will save money. The NPT is influenced by downhole restrictions during tripping in and out. Real time drilling data (RTDD) is used to monitor the drilling operations. According to the information obtained through RTDD, downhole restrictions can be detected in advance. Taking proper counter measures as early as possible will avoid restrictions and decrease NPT, thus decrease the cost.

Hookload (HKL) is an important RTDD parameter. This parameter tells us that how much force in total is applied on the hook. Especially while tripping out through curved sections, HKL is an important parameter for monitoring downhole restriction such as stuck pipe and uncleaned borehole. Predicting normal HKL in curved section with side forces is the topic of this thesis. To reach this goal, both experiment and simulation work will be performed and evaluated.

In the experimental part, a well in the real world, the oil field, was downscaled to lab scale so that a proper physical model could be installed in the workshop. Based on the downscaling calculation, the setup is designed and a 2D setup draft was drawn. This setup could satisfy current experimental requirements. Meanwhile, the design also considered future research. With proper adjustment, the setup can test HKL with circulation, cutting transportation, and 3D tripping out.

In the simulation part, several friction models and torque-drag models were investigated and introduced. The mechanism of side force was also analyzed based on soft string model and stiff string model. A 2D discrete static model was derived. This model could calculate drag force in tripping out considering side force in curved pipe. This static model had a general formula which could be applied in arbitrary well sections. A case study showed it had the same accuracy as classic soft string models. A 2D discrete dynamic model was derived. This model also considered side force in curved section. A case study showed that this dynamic model was valid and could

create reasonable simulated HKL. A future step will be to use experimental results for adjusting and verifying this mathematical model.

Table of Contents

List of Figure

List of Table

1. Introduction

Energy supply keeps increasing all over the world. Meanwhile, energy demand increases even more. How to fill the gap between the supply and the demand is always a tough issue. Different solutions are proposed to solve this problem, but none of them have made revolutionary breakthrough. In current situation, the fossil fuel occupies the largest fraction of the energy consumption. To fill the gap between oil supply and demand, one solution could be to drill more wells and produce more crude oil. However, most of the easy and large reservoirs have already been produced. We have to search into deep water and in the Arctic area to explore new oilfields. The drilling operations in these regions will cost more due to harsh environment and insubstantial infrastructure. Therefore, how to control the investment during drilling operation? One important method is to reduce the non-productive time (NPT). Real Time Drilling Data (RTDD) includes stored information and becomes quite important. Hook Load (HKL) is one of many parameters among the RTDD data, especially when tripping in or out of the drillstring. Downhole restrictions often become an issue during this operation. By analyzing the abnormal behavior of HKL, restrictions can be identified. Operators can provide remedies to prevent downhole incidents as early as possible. In order to analyze downhole restrictions and abnormal behavior, first we need to understand the normal behavior of tripping-out.

Both experiment and numerical simulation can help us reaching the goal mentioned above. The experimental design is one important task. Currently, the research focuses on the influence of the side force during tripping-out of the drillstring. According to theoretical analysis, the side force is activated in the curved section. A closer evaluation of the build-up section is thus reasonable. Based on a real well drilled in the North Sea, the build-up section is chosen and downscaled to laboratory level. The downscaling calculation follows the general downscaling principle and considers limitations in lab. The whole setup is also designed with the consideration of possible applications and further requirements in future.

Simulation is another important task in present thesis. For better simulation, different friction models and torque-drag models must be investigated. Previous work at the department did not consider bend forces very well in the static or dynamic models. The mathematical model applied

in this master thesis will consider this issue in a proper way. Based on this mathematical model, a simulator will be created. This simulator will test cases based on the experimental design. The mechanisms of side forces will also be discussed. High stiffness is an additional reason of side force acting in the bottom hole assembly (BHA) when moving it through curved sections.

2. Previous work relevant with HKL

Present chapter will introduce previous work. Many approaches were trying to reveal the physical mechanism of HKL, including theoretical analysis, mathematical model, and laboratory work. The previous work will be introduced chronologically.

Johancsik, Friesen, and Dawson (1984) presented the soft string model, which was the first step of a full torque and drag model. This model assumed that the drag force should conquer gravity and sliding friction along axial direction of the drillstring. This model did not consider other forces such as viscous fluid forces. At that time, this model was widely used in the industry.

Eric Edgar Maidla (1987) finished the dispute about borehole friction assessment, and applied friction in a new manner for casing design. Laboratory experiments were executed to evaluate the friction factor. Test with water-based mud and three oil-based muds showed that the most common friction factor values were between 0.2 and 0.3.

Ho (1988) modified Johancsik' soft string model (Johancsik et al., 1984). The improved model considered drillstring stiffness, stabilizer placement, and borehole clearance. The model also combined high stiffness in the BHA. Therefore, this model could predict torque and drag more precisely.

Falconer, Belaskie, and Variava (1989) noticed that in deviated wells, the surface measured WOB and torque could be different from the downhole-measured parameters, and provided two equations describing wellbore rotary friction factor and sliding friction factor individually.

Eric E Maidla and Wojtanowicz (1990) set up a medium-scaled borehole friction simulator that had the capabilities to test dynamic filtration. The experiment showed that friction coefficients were affected by mud type, mud cake, lubricant addition in low-solid drilling fluid, and so on. The experiment also proved as for previously stated findings that the friction factor fell in between 0.2 and 0.3.

Quigley, Dzialowski, and Zamora (1990) set up a full-scaled simulator to test wellbore friction in high angle holes. In the appendix A in their paper, the friction coefficient model was introduced. This model developed two formulas of friction coefficient. One coefficient was for calculating

drag force, and the other one was for calculating torque. These two formulas were quite simple. Their paper could provide some suggestions for the later experimental design.

Cordoso Jr, Maidla, and Idagawa (1995) provided the concept of 'pseudo' mechanical borehole friction factor to detect early borehole problems. For analytical purpose, HKL curves during tripping-out in different downhole situations were introduced. The standard HKL tripping curve and the problem-free on-site HKL observation both indicated that the HKL initial peak existed. The HKL curves mentioned in this paper were very good suggestions for future work.

B. Aadnoy and Andersen (1998); (2001) presented a set of explicit analytical equations to model drillstring tension for hoisting and lowering of the drillstring based on the soft string model. These explicit equations could only be applied on specific well profiles. Using these equations, the total drag force in a well could be derived by summing drag forces from each section.

McSpadden, Brown, and Davis (2001) introduced a 3D model for tripping downhole tools in and out on a cable. Since the cable was relatively soft, this model was an alternative form of soft string drag-torque model. Five real cases were introduced in this paper, all of them showed that this method could predict drag force for tripping in and out with cables such as wireline and slickline very well.

Polak and Lasheen (2001) presented a paper about mechanical modelling of pipes in horizontal wells. This model was a stiff string model and considered pipe deformation based on the theory of large deflections of flexible bars. This model was used to study stresses and strains on two pipes that were tested in the field. The theoretical results were compared with the strains measured in the field. The comparison between mathematical model and theoretical model were in reasonable agreement.

Andersson, Söderberg, and Björklund (2007) collected several different friction models for sliding contacts, like dry, boundary and mixed lubricated contacts. These models could satisfy different conditions. This paper separated all the mentioned friction models into two categories. One category was for common friction models such as pure sliding and oscillating sliding contacts. The other category was for friction at small displacement between sliding contacts.

Mason and Chen (2007) improved the previous stiff string model by considering buckling and tortuosity effects, and obtained a relatively realistic model. However, these factors were only considered with very simple mathematical models.

Cayeux and Daireaux (2009) developed a new computer system for monitoring friction. This system would be used for early downhole problem detection. The RTDD would update automatically during the drilling process. This system also calculated HKL using the torque and drag model. This system were applied on site, and the result showed very good performance that some downhole problems could be predicted in time.

Mitchell and Samuel (2009) presented a comprehensive review of torque-drag models. This paper discussed why the torque-drag model worked well in most cases but no so well in other cases. It was determined that the soft string model should consider viscous shear forces.

B. S. Aadnoy, Fazaelizadeh, and Hareland (2010) presented a new 3D friction model. This model only contained two equations. One was for straight-inclined well section. The other one was for arbitrary curved well sections. When azimuth did not change, this 3D model could be applied into 2D case.

Fazaelizadeh, Hareland, and Aadnoy (2010) presented a paper about the application of a new 3D model by B. S. Aadnoy et al. (2010). This paper focused on different effects on the new 3D model. Some real cases were also analyzed.

Wu, Hareland, and Fazaelizadeh (2011) applied the finite element method to the analysis of torque and drag. The FEA program developed in this paper was verified by analyzing HKL and torque against several real cases. The result showed that the HKL calculation was accurate, and the torque calculation was acceptable.

Cayeux, Daireaux, Dvergsnes, and Saelevik (2012a); (2012b) developed a software for monitoring well behavior during drilling operations. This software kept calculating various physical forces acting on drillstring. This software collected RTDD data and compared the estimated factors. If the calculated physical forces did not agree with the observation from RTDD, it indicated that the

well situation had changed. This paper also introduced several real cases. All of these cases showed that this software exhibited successful applications on site.

Glomstad (2012) delivered in her master thesis some interesting HKL analysis. Her workout included two parts. Firstly, she programmed a mathematical simulator based on mass-spring model simulating tripping-out in problem-free wellbores. Secondly, a laboratory experiment involving tripping-out in horizontal wellbore was set up, and tested with different downhole situations, for example with or without circulation and washout geometry. By comparing the results from experiment and simulation, they matched with each other sufficiently well in trouble-free condition. With circulation, the results did not match with each other very well.

Mme, Skalle, Johansen, and Sangesland (2012) applied a similar mass-spring mode as Glomstad. In this model, the drillstring was idealized as a mass-spring chain. All the weight were concentrated in mass blocks and the springs were weightless. The mass blocks represented the initial force, weight, friction force and so on, while the springs represented the elasticity of the drillstring. The detailed mathematical model will be introduced in later chapter. The mass-spring model was also the foundation of the mathematical model applied in present thesis.

Bjerke (2013) analyzed in her master thesis downhole restriction based on HKL signatures in RTDD. Her work was based on the work by Cordoso Jr et al. (1995) concerning theoretical HKL curve during tripping. She suggested a new system of category to simplify HKL signatures in two types; fixed and moveable restrictions. Bjerke's thesis indicated it was important to divide HKL signatures based on physical explanations rather than restrictions.

Kristensen (2013) provided a HKL mathematical model in his master thesis, which was quite different from Bjerke (2013). This model focused on three forces acting on drillpipe. They were tension, friction, and acceleration. According to normal tripping-out HKL, the coefficient of each force was determined firstly, and then the model could predict HKL for a specific case with proper coefficient determined in previous step. This mathematical model was a semi-empirical model. The result showed the simulation did not match field data well. It was hard to observe the initial HKL peak.

Kamel and Yigit (2014) presented their research about rotary drilling in oil well. The mathematical model in this paper was a dynamic mathematical model considering Newton's second law. This model was a good example of the mathematical model applied in present thesis. The simulation results agreed with observation on site very well. Therefore, the model could optimize drilling parameters.

Sjøberg (2014) finished his master thesis on extending and testing HKL rig on bases of the already existing setup. The setup consisted of hoist system, normal-pressured mud circulation system, drillstring and BHA, cutting injection system, and control-monitor system. The experiment result showed that the setup simulated initial peak of HKL successfully in normal downhole situation. This HKL rig provided a very solid foundation for future tests.

Swahn, Johansen, Hovda, and Skalle (2014) wrote an unpublished document to introduce dynamic drag force model. This model consisted of a set of coupled second order nonlinear differential equations.

Xie (2014) improved the existing mathematical model of Swahn et al. (2014) to simulate tripping-out operations in deviated well, and focused on the initial peak sometimes observed in the HKL. The synthetic generated data points had higher data frequency than the real BPOS, thus generating smoother curves and making curve fit operations more reliable. With the real BPOS as input in the mathematical model, the output, i.e. the simulated HKL curve, was not satisfactory.

Mitchell, Bjorset, and Grindhaug (2015) presented a new stiff string model. This model considered that the drillstring position corresponded with the minimum-curvature wellbore only at tool joints. Therefore, the drillstring obtained an additional degree of freedom (DOF). This additional freedom could describe bending moment. This paper also provided a real torque case. It indicated the result was fair.

3. Experimental design

One purpose of present thesis is to design an experimental test of HKL involving side forces. Two steps are necessary for this purpose. First, downscale the buildup section in a real wellbore to laboratory scale. Second, design the setup based on the dimensions and practical limitations of the laboratory wellbore.

3.1. Real case for experimental design

The real case we are interested in is a deviated well C-47 in Gullfask C. The relevant report was presented by Christophersen, Gjerde, and Valdem (2007). Figure 1 is the 2D well trajectory calculated on basis of survey data. This figure shows that the well trajectory includes four sections: vertical, buildup, tangent, and horizontal. Table 1 shows the main survey parameters of these four sections.
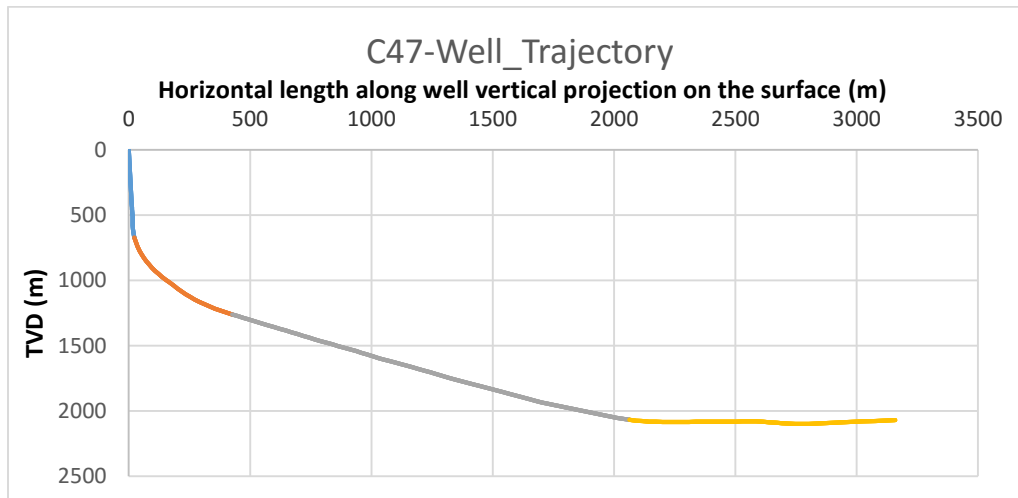
Figure 1: C47 well trajectory separated into 4 different sections based on the inclination.

Table 1: C47 well trajectory parameters.

Section	Horizontal	Slant	Buildup	Vertical
Section begin (m)	3238	1408.5	670	0
Section end (m)	4337.6	3238	1408.5	670
Section length (m)	1099.7	1829.5	738.5	670
Inclination lower end (∘)	91.5	63.3	61	1.3
Inclination upper end (∘)	91.5	63.3	1.3	0

Table 2 shows the detailed information about the drillstring. The real drillstring in well C-47 includes BHA, heavy pipe and normal drillpipe.

Table 2: C47 drillstring parameters drilling through the horizontal section.

Section	Horizontal BHA	Horizontal 5-in	Tangent 5-in	Tangent 6-5/8-in	Buildup 6-5/8-in	Vertical 6-5/8-in
Section length (m)	128.5	971.2	1150.5	679	738.5	670
Linear density (kg/m)	72.52	31.06	31.06	43.76	43.76	43.76
Section weight (kg)	9317	30165	35734	29714	32316	29319
Cross section (mm^2)	8106	3401	3401	4593	4593	4593
Elastic factor (N/m)	13881217	770432	650355	1488115	1368279	1508149

3.2. Downscaling the buildup section in a real wellbore

The experimental setup in the lab is based on the well defined above. For experimental design purpose and due to the space limitation in the laboratory workplace, Well C-47 have to be downscaled to proper dimensions so that the equipment in the workspace can be set up. Meanwhile, the experiment in the lab should simulate what happens in field as accurate as possible. The experiment will be designed to simulate tripping the drillstring out through the buildup section. The downscaling calculation and experimental design focus only on the buildup section. The following description is about the major equipment in this experiment, and about how these equipment simulate components in a real case.

- A bent steel pipe in the lab represents the buildup section in a cased hole. A casing with relatively small diameter can be processed with bending machine to create the curvature.
- A mass-spring chain in the lab represents the real drillpipe in the buildup section including elasticity. A drillpipe with smaller diameter can be cut into several pieces of mass blocks. The mass blocks simulate weight and inertia force of the drillpipe, and springs with proper stiffness linked between two neighboring mass blocks simulate elasticity. The mass blocks and springs can be welded together or linked with some kind of mechanical gadget.
- Wirelines will be attached at the upper and the lower end of this mass-spring chain, representing the remaining part of drillstring. The wireline will simulate the elasticity of the drillstring. At the upper end, the wireline will be linked to the mass-spring chain and

the winch providing the drag force. At the lower end, the wireline will be linked to the mass-spring chain and a huge mass block.

- A huge mass block represents the weight of drillstring below the buildup section.
- A winch represents the top drive system which is responsible for tripping out the drillstring.

The downscaling result is calculated both in a spreadsheet and in MATLAB program. The spreadsheet is used for pre-processing the wellbore trajectory data. Programming in MATLAB calculates the pulling-out force based on classic soft string model and a discrete static model which is going to be introduced in Chapter 5.2.1. The following bullets introduce the detailed procedures and the relevant explanations.

1. *Obtaining original information*

The first step is to obtain the relevant information of the buildup section in Well C47 and create a new spreadsheet. The relevant information includes survey data along the buildup section, dimensions of the wellbore, type of the casing cemented in this section, and type of the drillpipe being tripped through this casing. The relevant information is listed in Table 3.

Table 3: Basic information of the buildup section of Well C47.

OpenHole		
MD	668	m
hole size	24	in
Casing		
OD	20	in
Grade	N-80	grade
Weight	133	ppf
ID	18.73	in
DP 6-5/8 in		
OD	6.625	in
Weight	29.41	ppf
ID	5.965	in

2. Calculating the 2D well trajectory

Based on the survey points obtained in the first step, a 2D well trajectory is calculated, i.e. expand the 3D well trajectory into a vertical plane along the wellbore. There are two reasons for only considering the 2D well trajectory.

- Azimuth almost keeps constant in the buildup section in this case.
- The mathematical model applied in present thesis is a 2D dynamic model.

Therefore, it is reasonable to keep the experiment and the mathematical model in 2D so that they can easily verify each other. This mathematical model will only simulate tripping out operations.

3. Downscaling the wellbore to proper dimensions

This section demonstrates how to downscale the full-size wellbore to a proper dimension so that this wellbore, i.e. a bent steel pipe, can be assembled in the lab. After downscaling, the steel pipe assembled in lab is around 10 meters with the same shape as in the full-size wellbore. The downscaling factor equals to 10-meter bent pipe divided by the measured depth of the buildup section on site. In this case, the downscaling factor is 66.8. Figure 2 shows the well trajectory after downscaling.
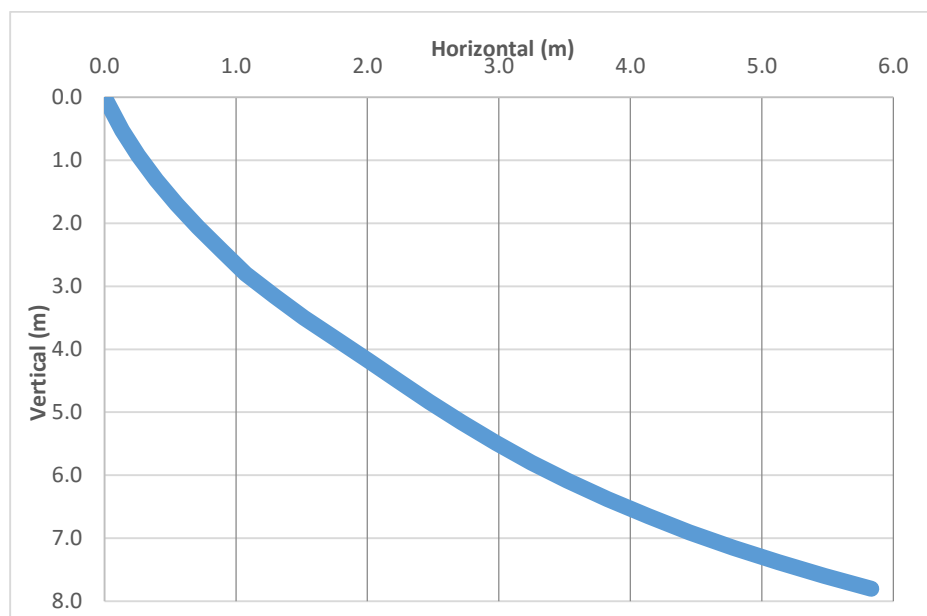
Figure 2: Lab well trajectory after downscaling.

11

The general principle of downscaling or upscaling requests changing all dimensions simultaneously. For a cubic model, if the length of this model decreases 10 times, then the height and width should also decrease 10 times. In this case, the diameter of casing is too small compared with the length. If the diameter of the casing decreases with the same downscaling factor, the pipe will be so small that nothing can pass through it, not to mention a proper mass-spring chain. Therefore, the experimental design only consider downscaling the casing and the drillpipe in length, not in other dimensions. This simplification will bring some challenges and it will be discussed later.

4. Downscaling the drillstring to proper dimensions

Applying the same downscaling factor, the drillpipe and the casing will have the same length. It will cause the mass-spring chain to move out of the casing at the beginning of the tripping out operation. The normal situation on site is that only one stand will be tripped out in one operation, i.e. around 30 meters. Apply the same downscaling factor to the tripping-out distance, a reasonable tripping-out distance in the lab should be 0.5 meter. Therefore, we would better decrease the length of the mass-spring chain so that after tripping out the mass-spring chain is still inside the bended pipe.

With the same downscaling factor, the mass-spring chain will have the same length as the casing. If the mass-spring chain becomes shorter, a heavier drillpipe should be applied, because the total weight of mass-spring chain should be kept constant. For example, a 680-meter 2-3/8 inch drillpipe is downscaled to a 10-meter drillpipe. If a 2-7/8 inch drillpipe substitutes this 2-3/8 inch drillpipe, 7.1-meter 2-7/8 inch drillpipe will be enough to keep the total weight constant.

5. Downscaling the elasticity coefficient

The correct elasticity coefficient of a drillstring after downscaling equals to the original elasticity coefficient divided by the downscaling factor. Based on this principle, the spring with the correct elasticity coefficient can be calculated. Elasticity coefficient is an external parameter evaluating the rigidity of an object. According to the explanation in previous steps, only the length of drillpipe need to be downscaled. If we only do so, the elasticity coefficient of this drillpipe will increase a lot, since the cross sectional area is still very large. This parameter is not consistent as

in the field conditions. An available solution is like this: Since the elasticity coefficient of the drillpipe increases a lot, it is reasonable to regard the drillpipe with high elasticity coefficient as a rigid body, then the drillpipe can be cut into several pieces as the 'mass' in mass-spring chain. Springs with proper elasticity coefficient compensate the rigidity of 'mass', and finally form the mass-spring chain.

6. Calculating the static drag force

This step calculates the static drag force in the field and in the lab. Since the drillpipe is only downscaled in length and the well trajectory does not change, the drag force in the lab should equal to the field drag force divided by the downscaling factor.

7. Calculating the normal force

This step calculates the normal force on site and in the lab. In previous step, drag forces at the upper and the lower ends are calculated, then the normal force can be calculated on basis of well trajectory. This calculation is programmed in MATLAB. The purpose of this calculation is to verify the direction of the normal force. If the resultant normal force is negative in the buildup section, it indicates that the drillstring is attached to the upper side of the casing and thus indicates the side force exists, and vice versa. The calculation shows that the resultant normal force is negative, i.e. the mass-spring chain is attached to the upside of the casing. The experimental model can test the side force in the bent pipe.

8. Calculating the weight of mass block

This step calculates how heavy a huge mass black should be to generate enough tension at the lower end. Depending on how the pulley system is, the mass block should at least generate enough tension equal to the calculation in step 6. In the spreadsheet, a suggested weight of mass block is given assuming a mass block is suspended at the lower end of a fixed pulley as shown in Appendix A.

9. Calculating the tripping-out distance

Generally, one stand will be dragged out in one tripping-out operation. The length of a real stand is about 30 meters. Considering the model only shrinks in length, the tripping distance in the lab

equals to the tripping out distance in the field divided by the downscaling factor. The result is about 0.5 meter in this case.

10. Calculating the tripping out velocity

A reasonable average tripping out velocity recorded in RTDD is about 0.2 m/s. Based on the principle mentioned in previous step, an average velocity in lab should be about 0.003 m/s.

The above procedures are the details and explanations of how to downscale a drillstring and a casing in the buildup section. Based on this procedure, all the calculations are performed in the spreadsheet and programmed in MATLAB. In Appendix D, the calculations consider five drillstrings with different grades while tripping-out in a cased hole in the buildup section.

3.3. Experimental setup and illustration

Experimental design is the main task of this thesis. The purpose of this experiment is to test HKL during tripping-out operations in bended sections. This experiment will also be used to verify the improved mathematical model in present thesis. Furthermore, the experiment should have potential for future research. With proper adjustment, the setup can test HKL in different scenarios. Currently, the setup is a little bit redundant for this experiment.

The setup has been downscaled on basis of the previous introduction. The experimental setup draft is attached in Appendix A. All the parts in this draft are marked with numbers. This subchapter will introduce the details and explanations about every part mentioned in the setup draft. Students who responsible for assembling equipment will have a better understanding after reading through this subchapter. The explanation for each component will be in numerical order, consistent with the serial numbers in the draft.

1. Curved pipe

The curved pipe simulates the buildup section. The length and the inclination of this pipe are designed based on the previous downscaling calculation. In reality, the buildup section in Well C47 is a cemented casing. A casing with proper diameter and curvature is therefore the choice. Picking out a casing with proper diameter is not a difficult task. The difficulty is that this casing should be bended by means of the bending machine. The bending will change the curvature of

the casing into the predicted value. If the casing after the metalwork cannot have exactly the same inclination as predicted, the inclination should be measured again, and then updated in the simulator.

2. Transition pipe

The transition pipe is a short pipe connecting the curved pipe and the horizontal pipe. According to the calculation, the inclination at the lower end of curved pipe is not horizontal. The short transition pipe will turn the inclination into horizontal and then connect to the horizontal pipe.

Another function of this transition pipe is to avoid unnecessary friction between the wireline and the pipe. An ideal scenario is that only the mass-spring chain is in contact with the upper side of the buildup section. However, as can be seen in Appendix A, the wireline may contact the upper side of the transition pipe during tripping-out. If the normal force in this section is high enough, it will generate high friction. This high friction is difficult to simulate since the mathematical model applied in present thesis can only simulate the friction created by the mass rather than the spring.

3. Horizontal pipe

The horizontal pipe is an extension of the curved pipe. Currently, it has no contribution to this experiment, but will be meaningful in future research. So far, the experiment and mathematical model only consider about 2D scenario, i.e. only consider inclination change. In reality, azimuth change must be a factor to be considered, because the azimuth change will also contribute to the side force. A horizontally curved pipe to test side force caused by azimuth change in future research will substitute this existing straight horizontal pipe.

4. Mass-spring chain

How to make the mass-spring chain and the relevant calculations have already been introduced in Chapter 3.2. It will not be repeated here.

5. Fixed pulley system assembled on scaffold

There are two sets of fixed pulley system in the draft. One set is assembled on a scaffold marked as term No. 18 in Appendix A, which is close to the upper end of the curved pipe. It will change

the wireline direction and guide the wireline back to the winch on the floor. The other one is installed on a scaffold marked as term No. 19 hoisting the mass block marked as term No. 11. The pulley in the draft is a fixed pulley system. Depending on detailed requirement, the fixed pulley system can be substituted into a travelling pulley system.

6. Velocity gauge

Two velocity gauges will be installed in the setup. One is close to the winch marked as term No. 17, and the other one is close to the mass block marked as term No. 11. The one close to the winch will test tripping-out velocity at surface, and then transfer it into tripping-out distance, i.e. the BPOS. The other velocity gauge will only record the velocity of the huge mass block. The record from this velocity gauge will not be used as the input, but will be compared with the simulated velocity at this point to verify the mathematical model.

7. Load cell

Similar to the velocity gauge, two load cells will be installed in the setup. The one close to the winch marked as No. 17 will test tripping-out load at surface, i.e. simulating the HKL in reality. The other one close to the huge mass block will test the tripping-out load at bottom. The records from both load cells will be compared with the simulated load to verify the mathematical model.

8. Fixed pulleys assembled on surface

Just as the fixed pulley system assembled on the scaffold marked as term No. 18, the surface pulley are responsible for changing the direction of the wireline.

9. Wireline with specific elasticity

The main function of the wireline is to pull the mass-spring chain and the mass block. Meanwhile, the elasticity of the wireline should be considered. These two wirelines can be regarded as two very long springs. The elasticities have to be measured correctly as the input to the simulator.

10. Fluid piping

The fluid pipes connect all the circulation equipment. It will not attribute to this experiment, but will be necessary in future research when the experiment considers tripping-out combined with the circulation or the cutting transportation.

11. Mass block

The mass block simulates the rest of the drillstrings below the buildup section. The weight of this mass block has been calculated based on the downscaling principle. In fact, the weight of this block should not be exactly same as calculated value, but should be close. The mass block should be heavy enough to create enough tension so that the mass-spring chain will be forced in contact with the upper side in the curved pipe.

12. Flowmeter

The flowmeter is for future research. When drilling fluid circulation is considered in the wellbore, fluid flow rate should be recorded.

13. Two-phase separator

This equipment is for future research. When considering borehole-cleaning issues, cuttings will be added into the circulation. After circulation, the separator will filter the cuttings from the drilling fluid.

14. Mud tank

After the separator, the drilling fluid will be stored and mixed with the rest of the mud.

15. Cuttings tank

After the separator, the cuttings will be stored in a tank.

16. Mud Pump

The mud pump provides liquid mass flow.

17. Winch & Motor

The winch and the motor have the same function as the drawworks on a drilling rig. It provides hoisting power for tripping out the drillstring. The motor should have the ability of adjusting the output power so that the tripping-out velocity can be controlled precisely.

18. Scaffold supporting curved pipe

The scaffold is a huge steel frame that is strong enough to support the curved pipe, and to decrease the vibration caused by the tripping-out operation. The scaffold can be wide enough so

that several pipes with different shapes can be assembled in parallel, which is convenient for future tests.

19. Scaffold supporting mass block

The scaffold supports the pulley system for hoisting the mass block.

20. Pipe T & seal

In future research, when fluid circulation is considered, the pipe T and the seal should be assembled at the upper and the lower ends of the curved pipe. The pipe T has three outlets. One connects the end of pipe, the second one connects the circulation pipe, and the third one is plugged with a seal to avoid drilling fluid leaks. A proper hole with isolation material through this seal allows wireline move freely.

This subchapter concludes the detailed instruction for every part mentioned in the setup draft. It will be helpful for setting up more experiments in future research.

4. Friction model and side force analysis

This chapter will focus on different friction models and the mechanism behind the side force. How to calculate the friction is always important in torque-drag models. Most commonly, a constant friction coefficient, i.e. Coulomb friction model, is applied. Besides the constant friction model, other friction models will be introduced in this chapter, which can be applied in future research. In the last part of this chapter, the side force is briefly analyzed and discussed.

4.1. Friction models

The friction always have strong impact on the drilling operation. This brief introduction is mainly based on the discussion by Andersson et al. (2007) and on other models applied in the industry. At the end of this section, a friction correction factor for tripping-out operations through a cased hole will be introduced.

4.1.1. Coulomb friction model with dynamic and static friction coefficients

The Coulomb friction model is always applied in dry friction scenarios. This model only considers a constant friction coefficient. The HKL should overcome the static friction and enable the drillstring to move upwards. With a specific HKL, the velocity of the drillstring is either constant, in acceleration, or in deceleration. Equation (1) and (2) are the Coulomb friction model in static and dynamic scenarios respectively.

$$F = fF_N sign(v) \tag{1}$$

$$F' = f'F_N sign(v) \tag{2}$$

$sign(v)$ in Equation (2) is the sign function of the tripping-out velocity defined as follow:

$$sign(v) = \begin{cases} -1 & \text{if } v < 0 \\ 0 & \text{if } v = 0 \\ 1 & \text{if } v > 0 \end{cases} \tag{3}$$

In mathematics, the sign function is an odd mathematical function that extracts the sign of a real number. This function indicates that the direction of the friction is always opposite to the direction of the velocity. Figure 3 shows that the $sign(v)$ function is not a continuous function.
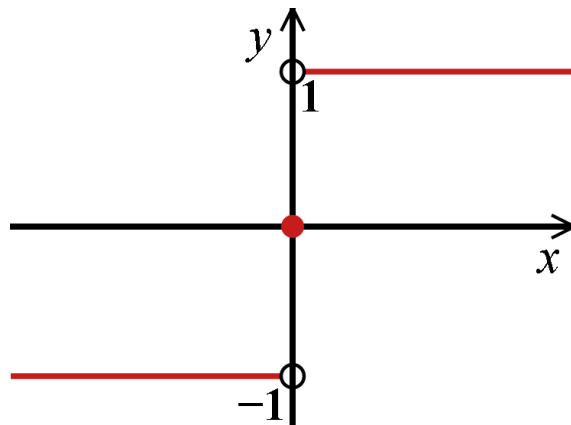
Figure 3: Discontinuous sign function (Wikipedia, 2015).

The difference between the dynamic friction coefficient f' and the static friction coefficient f is seen in Equation (4) and in Figure 4.

$$f' < f \qquad (4)$$
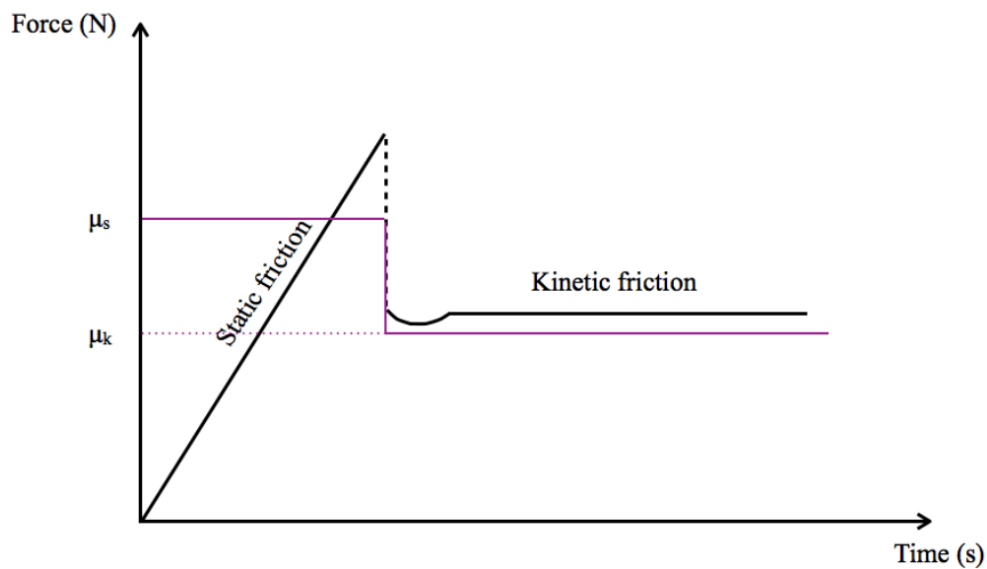
Figure 4: The static and the dynamic friction coefficients (Glomstad, 2012).

Vibration causes the sliding direction change, which in tern leads to change in the direction of friction. The $sign(v)$ function in the Coulomb friction model is used for describing friction direction change. The disadvantage of this function is that the simulator will be unstable since the function is not continuous. The continuous function $\tanh(k_{tanh}v)$ can be applied to solve this problem with the disadvantage of increasing the computing time. k_{tanh} determines how quickly this function reaches -1 or $+1$ with respect to the velocity.

The literature published over the last five years showed that the Coulomb friction model is still the primary friction model applied in the torque-drag model. The friction coefficient should first match the field observation, and can then be input into the simulator. Another interesting issue is that the running-in friction coefficient always differ from the tripping-out friction coefficient. This fact indicates that the constant friction coefficient is a very general parameter to describe the overall friction situation in the wellbore. The constant friction coefficient does not necessarily indicate that the friction follows the Coulomb friction behavior.

4.1.2. Viscous friction model

The dynamic friction model is more or less nonlinear. In a dynamic situation, the viscous friction model can be applied. This model is described through Equation (5) by Andersson et al. (2007).

$$F = k_v v$$
(5)

Generally, the validity of the viscous friction model is doubtful except for some specific cases. In full film contact, the viscous model might represent the friction behavior reasonably. While in other situations, it is difficult to describe the friction acceptably with this viscous model.

4.1.3. Combining the Coulomb friction model and the viscous friction model

Both the Coulomb friction model and the viscous friction model have their own limitations. A combination of these two models is a reasonable choice, expressed through Equation (6).

$$F = \begin{cases} F_c \min(k_{sat}v,1) & \text{if } v \geq 0 \\ F_c \min(k_{sat}v,-1) & \text{if } v \leq 0 \end{cases}$$
(6)

Andersson et al. (2007) used MATLAB/Simulink to test this model. The result shows that this model is a good friction model for sliding and oscillating modes.

4.1.4. The Stribeck friction model

Drilling operations always require fluid circulation. In such situations, the sliding contact, i.e. the interface between drillstring and wellbore, is lubricated with the drilling fluid. This friction model is developed by Stribeck (1903) and the detailed description of this model is presented as follow: The friction decreases as the sliding velocity increases at the initial moment. Then the sliding contact changes into the mixed or full film condition. In this stage, the friction can be constant, increased or decreased depending on sliding velocity and on basis of viscous and thermal effects.

The Stribeck friction model is still very popular nowadays even though other breakthroughs have been made in this area. Therefore MathWorks (2015) developed a toolbox for this classic method. The typical formula can be written as:

$$F = \left(F_c + \left(F_{break} - F_c \right) e^{\left(-c_v |v| \right)} \right) sign(v) + f v \qquad (7)$$

Just like the discussion in the Coulomb friction model, the function $sign(v)$ can be replaced by the function $\tanh\left(k_{\tanh} v \right)$ to accommodate the sliding direction change. With the proper parameters, the Stribeck friction model can describe the relation between the friction and the sliding velocity very well. The Coulomb friction model with the constant dynamic and static friction coefficients can be regarded as a simplification of the Stribeck friction model. Figure 5 is presented by MathWorks (2015), and shows the detailed friction change with respect to the increase of the sliding velocity.
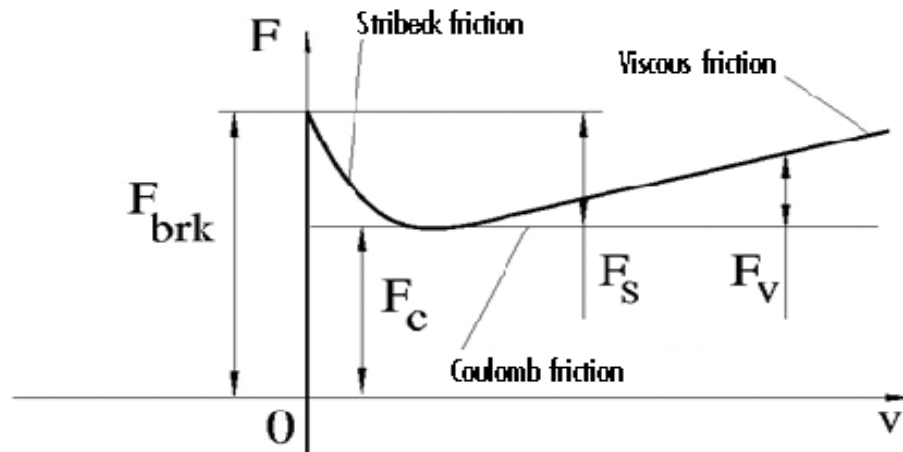
Figure 5: Stribeck friction model (MathWorks, 2015).

4.1.5. Friction factor defined by Maidla and Wojtanowicz

Eric E Maidla and Wojtanowicz (1990) developed a definition of the borehole friction factor. With the HKL observed on site and the calculation based on the well trajectory, this borehole friction coefficient can be expressed by Equation (8).

$$\mu_B = \frac{\left| HKL - W_V \pm F_D \right|}{\displaystyle\int\limits^{D} w_N(l)\,dl} \tag{8}$$

4.1.6. Friction with the stochastic process

All the friction models mentioned above consider that the contact surfaces is smooth. However, the contact surface in any wellbore is quite complex. From downhole videologs in Figure 6, it is clear to see how tough the naked wellbore is. Even in a cased hole, considering cutting transportation, the contact surface is not always as smooth as in ideal situations. Friction on this contact surface is caused by stochastic interactions between rubbing asperities. Rubbing asperity means the contact surface is not absolute smooth, and leads to friction by shearing the surface materials, coating, or lubricants (Andersson et al., 2007).

Figure 6: Wellbore is not ideally smooth ("Well Integrity Inspection," 2015).

Actually, in most real cases, the friction is more or less stochastic, but most of the friction models just use the average friction values to instead of the stochastic values. The stochastic friction model can be derived by adding a stochastic friction term to the smooth friction model. The general model is presented in Equation (9).

$$F_{stoc} = F_{smooth} + S\left(A, frq\right)$$

(9)

The stochastic friction term can be determined experimentally.

4.1.7. Effect of Contact Surface

Eric E Maidla and Wojtanowicz (1990) discussed the contact surface correction factor during tripping-out operations. When a drillpipe moves through a curved surface such as a buildup section of a well, the drag force caused by the normal force applied on the contact surface can be determined by Equation (10).

$$F_D = C_s \mu F_n$$

(10)

For approximate evaluation, the correction factor can be defined in Equation (11).

24

$$C_s = \frac{4}{\pi}$$
(11)

The correction factor C_s varies between 1 and $4/\pi$ depending on the contact surface angle γ. Equation (12) presents the correction factor based on the surface angle.

$$C_s = \frac{2}{\pi} \gamma \left(\frac{4}{\pi} - 1 \right) + 1$$
(12)

The detailed derivation of C_s was presented by Eric E Maidla and Wojtanowicz (1990). The contact surface is defined by the length of an arc between interception points of the two circles. The larger circle is the casing or the formation. The smaller circle is the tubing or the drillstring. Initially, these two circles are internally tangent with each other, and then the smaller circle such as the drillstring will be deformed by the side force. Figure 7 is presented by Eric E Maidla and Wojtanowicz (1990) and shows the physical meaning of the surface contact.
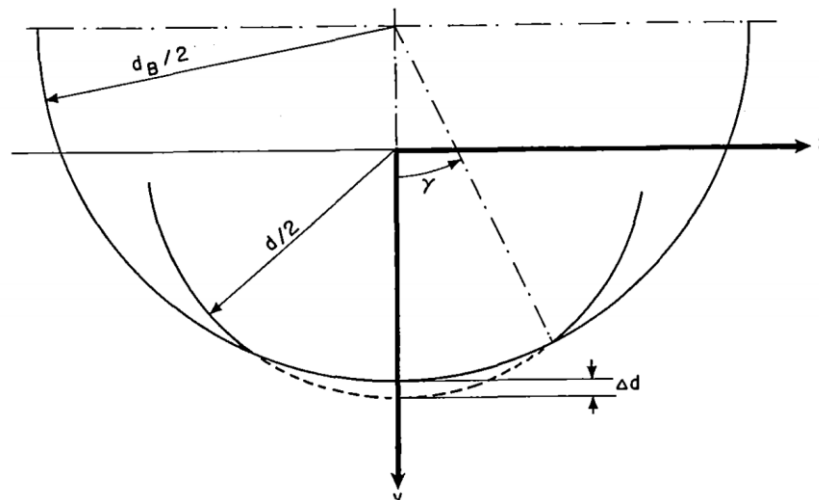
Figure 7: Surface of contact (Eric E Maidla & Wojtanowicz, 1990).

4.2. Discussion about the side force

4.2.1. Geometry stiffness

The mathematical model applied in present thesis is a combination of the mass-spring model and the force analysis with orthogonal decomposition. The drillstring is regarded as a soft string. It

means the stiffness of the drillstring will not be considered, i.e. the drillstring is soft. In most of the real cases, this assumption is correct, because the drillstring is thousands of meter long and the azimuth and inclination change seldom abruptly. The string tension will be the only reason causing side force when the well path changes its orientation. Figure 8 is an illustration of this theory by Larsen (2015).
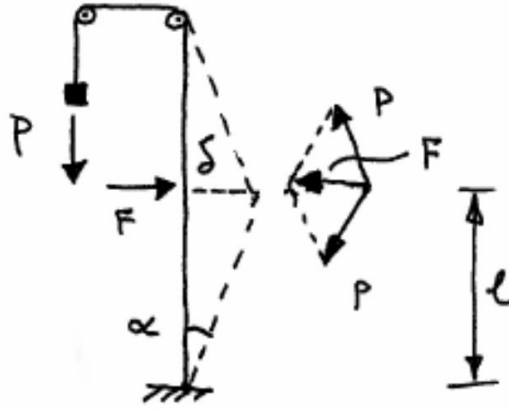
Figure 8: Drag force causes side force considering soft drillstring (Larsen, 2015).

From Figure 8, we can derive the geometric stiffness factor. The side force F at the lateral direction is the resultant of the tension or drag force P. When the deflection angle α is known, F can be written as

$$F = 2P\sin\alpha \tag{13}$$

Consider the deflection angel is very small, the following assumption is reasonable.

$$\sin\alpha \approx \alpha \tag{14}$$

And α is defined as

$$\alpha = \frac{\delta}{l} \tag{15}$$

Therefore, the side force becomes

$$F = 2P\frac{\delta}{l} = \frac{2P}{l}\delta = K_G\delta \tag{16}$$

Where the geometry stiffness is defined as

$$K_G = \frac{2P}{l} \qquad (17)$$

Similar analysis has been applied in the mathematical model of this thesis.

4.2.2. Bending force

The BHA always has high stiffness. The high stiffness indicates that this part of the drillstring is not 'soft'. It is reasonable to consider bending forces in the high-stiffness string such as in the BHA. The textbook, Mechanics of Materials by Hibbeler (2010), presented the beam stiffness theory. One scenario of this theory shown in Figure 9 describes that the concentrated normal force applied in the middle of the beam. This scenario is quite similar with what happens in the drillstring when the drillstring is forced to attach the wall of the wellbore during the tripping through a bend or a dog-leg. P in Figure 9 is the concentrated normal force. In the beam stiffness theory, the maximum deflected angel is derived from the concentrated normal force. For a drillstring, the survey data measures the inclination change. According to the inclination change, the maximum deflected angel for a specific drillpipe can be determined, then the normal force P will be derived accordingly.
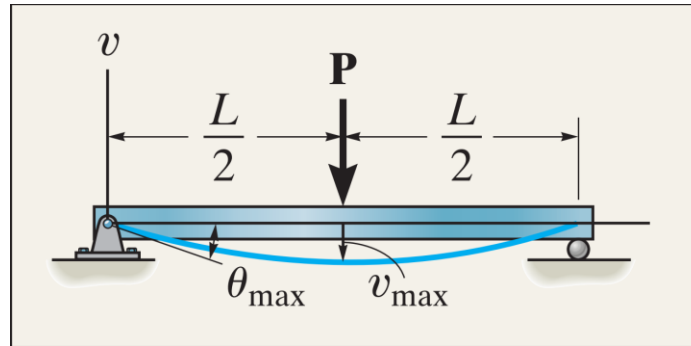
Figure 9: Concentrated bending force causes beam bent (Hibbeler, 2010).

The following equations are the detailed derivation in the 2D situation:

The inclination change between two neighboring survey points is as follows:

$$\Delta\theta = \theta_2 - \theta_1 \qquad (18)$$

27

Assume the side force is concentrated in the middle of this string, and then the maximum inclination changes at the two ends are equal to each other.

$$\theta_{endpo\,int} = \frac{\Delta\theta}{2} \tag{19}$$

The deflection angel in this scenario.

$$\theta_{endpo\,int} = \frac{-PL^2}{16EI} \tag{20}$$

Because $\theta_{endpo\,int}$ is known, the normal force caused by bending is:

$$P = \frac{16\theta_{endpo\,int}EI}{-L^2} \tag{21}$$

Here we only consider the absolute value, and substitute the expression for the maximum deflection angle. The side force is:

$$P = \left| \frac{8\Delta\theta EI}{-L^2} \right| \tag{22}$$

When any part of a drillstring with high stiffness is forced to attach the wall of the well, the additional side force in Equation (21) can be considered. In normal situations, i.e. in the soft string model, only the side force caused by the geometry stiffness need to be considered.

5. Mathematical models

This chapter will introduce several torque-drag models developed in the recent thirty years, and then introduce the models applied in present thesis. All of these mathematical models can solve the drag force during tripping operations. For the models developed in previous works, a brief introduction with important formulas will be shown. For the models applied in present thesis, a detailed explanation and derivation will be given. The mathematical models applied in present thesis are the fundament of the programming in Chapter 6. The author will introduce all the models chronologically.

5.1. Torque and drag models developed previously

5.1.1. Soft string model

Johancsik et al. (1984) introduced a soft string model. This model assumed that the axial friction and the weight of the drillstring were causing the drag force and the side force. The axial friction is induced by gravity, normal force and tension caused by gravity. An equation to calculate the 3D normal force was also provided in their paper. This method is one of the first contributions to understand the drag force in an arbitrary wellbore. Figure 10 shows the forces applied in the soft string model including the drag forces at the two ends, the normal force, and the friction force caused by the normal force. The side force part comes in Chapter 4.2.1.
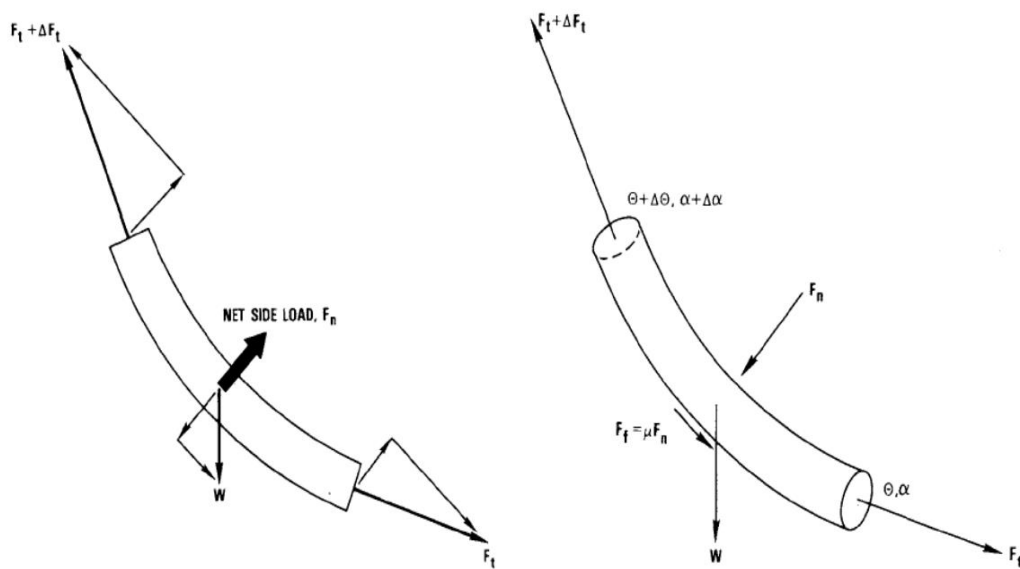
Figure 10: The forces applied in a soft string model (Johancsik et al., 1984).

As can be seen in Figure 10, the pipe represents one joint of the drillstring. In order to calculate the total force during tripping-out, i.e. the HKL, it is better to calculate the drag force from the bottom to the top of the well. The resultant force at any section is governed by the Equation ((23).

$$F_t + \Delta F_t = F_t + W\cos(\bar{\theta}) + \mu F_n \tag{23}$$

Equation (24) defines the normal force.

$$F_n = \sqrt{\left[F_t \Delta\alpha \sin(\bar{\theta})\right]^2 + \left[W\sin(\bar{\theta}) + F_t\Delta\theta\right]^2}$$
$$\bar{\theta} = \frac{\theta_{t+\Delta t} + \theta_t}{2}$$
$$\Delta\theta = \theta_{t+\Delta t} - \theta_t$$
$$\Delta\alpha = \alpha_{t+\Delta t} - \alpha_t \tag{24}$$

This model is simpler than the later developed mathematical models, but the concept of the soft string developed in this model is meaningful for future research and application in the industry.

5.1.2. 2D and 3D borehole friction model developed by Maidla

Eric Edgar Maidla (1987) presented a general method to predict the drag force. This method has two sets of equations applied in the 2D and the 3D case, separately. Both sets are based on the analytical description of the well profile. The following factors are considered in this model:

- Spatial changes
- Buoyancy effect
- Coulomb friction model
- Hydrodynamic friction
- Effect of the pipe-borehole contact surface

However, the torsion and the spring effects are not considered in this model. The 3D model is like this:

$$\frac{dF_A}{dl} = q_U(l) \pm \mu_B C_S(l) q_N(l) \tag{25}$$

and

$$q_N(l) = \sqrt{q_b(l)^2 + \left[q_p(l) + \frac{F_A(l)}{R(l)}\right]^2}$$ (26)

where

$$q_U(l) = \vec{q} \cdot \vec{u}(l)$$
$$q_b(l) = \vec{q} \cdot \vec{b}(l)$$ (27)
$$q_p(l) = \vec{q} \cdot \vec{p}(l)$$

$$R = \frac{l_i - l_{i-1}}{\arccos\left[\cos(\theta_i - \theta_{i-1}) \cdot \sin\alpha_i \cdot \sin\alpha_{i-1} + \cos\alpha_i \cdot \cos\alpha_{i-1}\right]}$$ (28)

The positive sign indicates upward movement, and vice versa. The vector products indicate that the pipe weight distribution on the trihedron coordinator at any point are based on the well trajectory. It is reasonable to apply the above 3D formulas at any survey point.

For the 2D case, the vector products in the above formulas will be simplified to become the explicit algebraic function, and the relevant equation is as follows:

$$F_{A_{i-1}} = AF_{A_i} + C_1 \cdot \frac{qR}{1 + \mu_B}\left[(\mu_B - 1)(\sin\alpha_{i-1} - A\sin\alpha_i) + 2C_2\mu_B(\cos\alpha_{i-1} - A\cos\alpha_i)\right]$$ (29)

$A = \exp\left[\mu_B(\alpha_i - \alpha_{i-1})\right]$ for tripping-out operations and $A = \exp\left[\mu_B(\alpha_{i-1} - \alpha_i)\right]$ for tripping-in operations. The constant C_1 and C_2 represent the sign functions depending on the location of the pipe in the build-up or the drop-off section. The radius of the bended section is as follows:

$$R = \frac{l_i - l_{i-1}}{\alpha_i - \alpha_{i-1}}$$ (30)

During the well planning stage, this 2D model is accurate enough for the casing design. It is the first time that a torque-drag model provided a method to analyze forces based on trihedron coordinator.

5.1.3. The explicit analytical model based on different well sections

B. Aadnoy and Andersen (1998) presented an explicit method for torque-drag calculation based on the soft string model. This method finally derived the different analytical equations for the different well trajectories with the different operations, for example, a specific equation for the

pulling force in the build-up section. Figure 11 and Figure 12 presented the forces and geometries in a straight hole and in a build-up section.
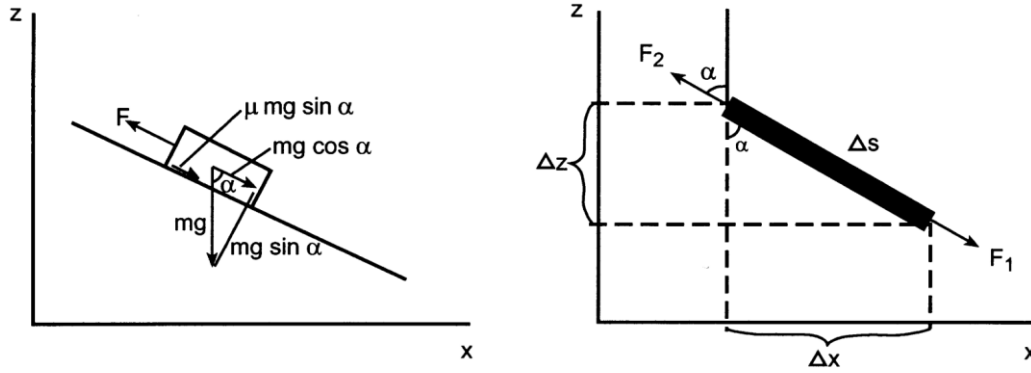
Figure 11: Forces and geometry in straight hole (Aadnøy & Andersen, 2001).
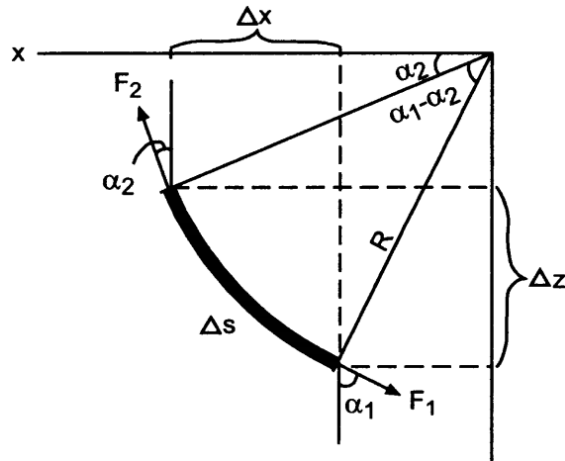
Figure 12: Forces and geometry in build-up section (Aadnøy & Andersen, 2001).

The formula for the pulling force in a straight inclined section is presented in Equation (31). This equation is also valid for the vertical section.

$$F_2 = F_1 + w\Delta s\left(\cos\alpha + \mu\sin\alpha\right) \tag{31}$$

For the build-up section, Equation (32) is applied, which is:

$$F_2 = F_1 e^{-\mu(\alpha_2 - \alpha_1)} - wR\left[\sin\alpha_2 - e^{-\mu(\alpha_2 - \alpha_1)}\sin\alpha_1\right] \tag{32}$$

Notice that this equation cannot be simplified into Equation (31), if the inclination at the upper end and the lower end are the same. It indicates that these two formulas only suit their own situation. Other equations in this model will not be presented here since they are not relevant to this thesis.

5.1.4. 3D analytical model for the wellbore friction

B. S. Aadnoy et al. (2010) developed a 3D model on basis of their previous work (1998). This model can predict the drag force in an arbitrary wellbore trajectory depending on two general equations. We will not express the torque equations (not relevant in present thesis). This model requires that the dogleg should be calculated first.

$$\cos\theta = \sin\alpha_1 \sin\alpha_2 \cos(\phi_1 - \phi_2) + \cos\alpha_1 \cos\alpha_2 \tag{33}$$

The equation of the drag force in straight inclined wellbores is the same as the equation used in the previous model, which is:

$$F_2 = F_1 + \beta\Delta l w(\cos\alpha + \mu\sin\alpha) \tag{34}$$

For the curved trajectories, a general equation will be applied.

$$F_2 = F_1 + e^{\pm\mu|\theta|} + \beta w \Delta L \left\{ \frac{\sin\alpha_2 - \sin\alpha_1}{\alpha_2 - \alpha_1} \right\} \tag{35}$$

where the positive sign indicates tripping-out, and vice versa.

5.1.5. Mass-spring model

Mme et al. (2012) and Glomstad (2012) developed this mass-spring model. They tried to create a reliable mathematical model matching field observations considering drillstring elasticity.

The mass-spring model discretizes the drillstring as a series of the mass components linked by springs between each pair of neighboring mass components. The mass components simulate the forces like gravity, friction, inertial force, buoyancy and fluid drag force, and the springs provide the elasticity. The physical model is described in Figure 13 by Glomstad (2012).
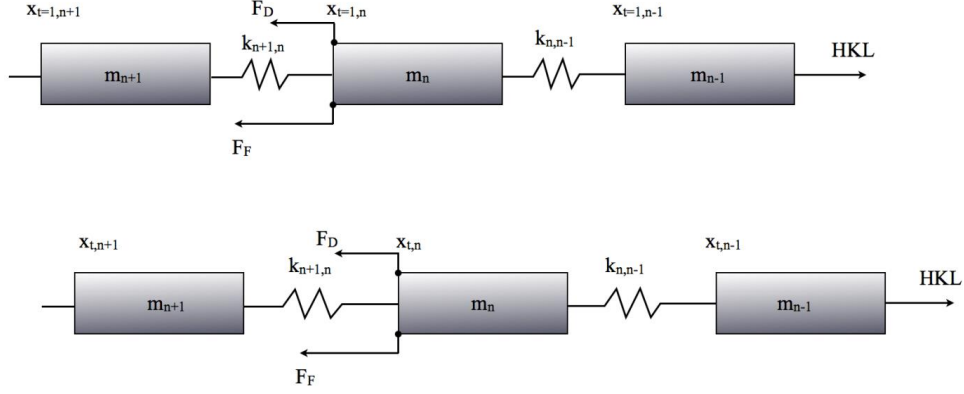
Figure 13: The draft of mass-spring model (Glomstad, 2012).

The upper string in Figure 13 describes the initial state of the drillstring, and the lower string describes the state after the first three mass components have been activated. During tripping-out, the drillstring is elongated due to the elasticity. The following set of equations represents the mass-spring model.

$$
\begin{cases}
m_1 a_1 = k_{12}(x_2 - x_1 - \Delta_{12}) - F_{f1} - F_{D1} \\
m_2 a_2 = k_{23}(x_3 - x_2 - \Delta_{23}) - k_{12}(x_2 - x_1 - \Delta_{12}) - F_{f2} - F_{D2} \\
m_3 a_3 = k_{34}(x_4 - x_3 - \Delta_{34}) - k_{23}(x_3 - x_2 - \Delta_{23}) - F_{f3} - F_{D3} \\
\vdots \\
m_{n-1} a_{n-1} = k_{(n-1)n}(x_n - x_{n-1} - \Delta_{(n-1)n}) - k_{(n-2)(n-1)}(x_{n-1} - x_{n-2} - \Delta_{(n-2)(n-1)}) - F_{f(n-1)} - F_{D(n-1)} \\
m_n a_n = HKL - k_{(n-1)n}(x_n - x_{n-1} - \Delta_{(n-1)n}) - F_{fn} - F_{Dn}
\end{cases}
\tag{36}
$$

In Equation (37), the acceleration term is derived from the second derivative with respect to the position of the mass block. x denotes the position of specific mass block.

$$
a = \frac{\Delta v}{\Delta t} = \frac{\Delta^2 x}{\Delta t^2}
\tag{37}
$$

Hook's Law describes the spring force in Equation (36). $x_{n-1} - x_{n-2} - \Delta_{(n-2)(n-1)}$ indicates the spring displacement. F_f indicates the frictional force. F_{Dn} indicates the fluidic drag force. Taking all the forces into the consideration, the HKL at time t is

$$
HKL^t = F_{weight} + F_{spring}^t + \sum_{n=1}^{N} F_{fn}^t + F_{D,BHAn}^t
\tag{38}
$$

34

Glomstad (2012) derived Equation (38) on basis of the same assumptions, such as the spring elasticity is always a constant, and the fluidic drag force only influences the BHA.

The author of this thesis also tried to derive an expression of the HKL from Equation (36). The method is to sum up all the equations, and then separate the term of HKL.

$$
\left.
\begin{aligned}
HKL^t &= \sum_{n=1}^{N} m_n a_n^t + \sum_{n=1}^{N} F_{fn}^{\ t} + \sum_{n=1}^{N} F_{Dn}^{\ t} \\
a_n^t &= \frac{\partial^2 x_n}{\partial t^2}
\end{aligned}
\right\} \rightarrow
$$

$$
HKL^t = \sum_{n=1}^{N} m_n \frac{\partial^2 x_n}{\partial t^2} + \sum_{n=1}^{N} F_{fn}^{\ t} + \sum_{n=1}^{N} F_{Dn}^{\ t}
$$

(39)

The acceleration changes in different mass components reflect the influence of the elasticity. The spring force is still there, just as the inner force. However, this model has a disadvantage. The gravity is the only reason for the friction. The well trajectory is not considered in this model.

5.1.6. Basic 2D discrete model

Sangesland (2012) presented a model in his lecture. In 2D situation, Sangesland developed one method with the orthogonal decomposition along the radial and the tangent direction, and established the force equilibrium in an infinitesimal drillstring element. Figure 14 illustrates the force decomposition.
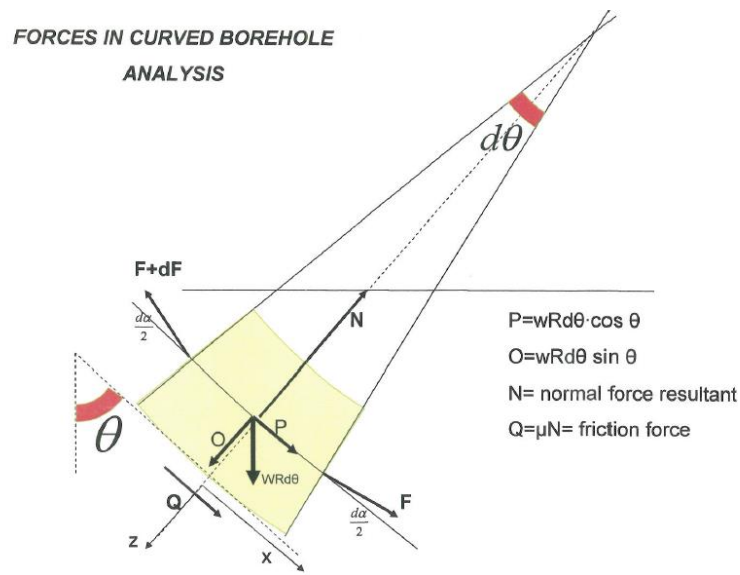
Figure 14: Force in a curved borehole (Sangesland, 2012).

This model decomposes the forces along x and z direction. Equation (40) describes the equilibrium along x direction.

$$\sum F_x = (F + dF)\cos\frac{d\theta}{2} - F\cos\frac{d\theta}{2} - Q - P = 0 \tag{40}$$

Along z direction, the equilibrium equation is

$$\sum F_z = N - O + (F + dF)\sin\frac{d\theta}{2} + F\sin\frac{d\theta}{2} = 0 \tag{41}$$

The following equations define the terms in above two equations.

$$
\begin{aligned}
P &= wRd\theta\cos\theta \\
O &= wRd\theta\sin\theta \\
N &= \text{normal force resultant} \\
Q &= \mu N
\end{aligned}
\tag{42}
$$

For this infinitesimal drillstring element, the inclination change should be very small; therefore, some reasonable assumptions will be

$$
\begin{aligned}
\cos\left(\frac{d\theta}{2}\right) &\approx 1 \\
\sin\left(\frac{d\theta}{2}\right) &\approx \frac{d\theta}{2} \\
\frac{dFd\theta}{2} &\approx 0
\end{aligned}
\tag{43}
$$

The above equations can be solved by substituting Equation (41) into Equation (40) to cancel term N.

There are two disadvantages in this discrete soft string model:

1. This model is a pure static analysis with the orthogonal decomposition. It does not include the acceleration of the drillstring. However, the tripping-out operation should be a dynamic process. Previous static torque-drag models also have this disadvantage.
2. This model does not consider elasticity.

5.1.7. 2D dynamic model considering drillstring elasticity

Swahn et al. (2014) developed a dynamic model considering the drillstring movement and the elasticity. This dynamic model is a hybrid of the soft string model and the mass-spring model. Like the mass spring model, this model discretizes the drillstring into mass blocks connected with the springs between each pair of blocks. For each mass block, this model utilizes orthogonal decomposition mentioned previously to analyze the forces. With the orthogonal decomposition, the resultant force along the radial direction is in an equilibrium condition. Along the tangent or axial direction, the resultant force will follow the Newton's second law, which is just like the left hand side in the mass-spring model in Equation (36). Therefore, this model can simulate the elasticity and have the ability to simulate side force in the buildup section. Figure 15 is the physical model.
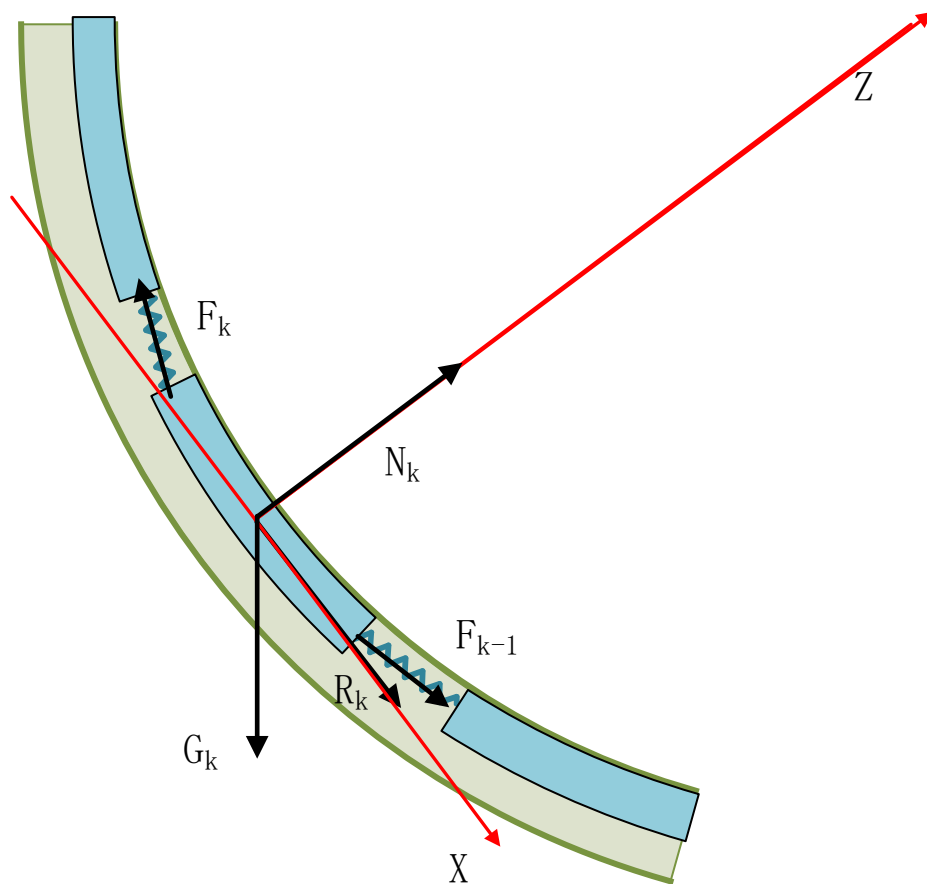
Figure 15: Schematic and stress analysis of dynamic model.

Equations (44) describe the result of the orthogonal decomposition at the component k.

$$F_{xk} = B_f m_k g \cos\left(\theta_k\right) + \mu N_k - \left(F_k - F_{k-1}\right)\cos\left(\frac{\Delta\theta_k}{2}\right) = m_k \frac{\partial^2 u_k}{\partial t^2}$$

$$F_{zk} = -B_f m_k g \sin\left(\theta_k\right) + N_k + \left(F_k + F_{k-1}\right)\sin\left(\frac{\Delta\theta_k}{2}\right) = 0$$

(44)

The terms $\cos\left(\frac{\Delta\theta_k}{2}\right) \approx 1$ and $\sin\left(\frac{\Delta\theta_k}{2}\right) \approx \frac{\Delta\theta_k}{2}$ have been approximated. Substitute F_{zk} into

F_{xk} to cancel N_k, and then obtain Equation (45).

$$B_f m_k g \left(\cos\left(\theta_k\right) + \mu\sin\left(\theta_k\right)\right) - \left(F_k - F_{k-1}\right) - \mu\left(F_k + F_{k-1}\right)\frac{\Delta\theta_k}{2} = m_k \frac{\partial^2 u_k}{\partial t^2}$$

(45)

The components $\left(F_k - F_{k-1}\right)\Delta\theta_k$ is assumed small and $\left(F_k - F_{k-1}\right)\Delta\theta_k \approx 0$. Then simplify the

Equation (45) and move the acceleration term to the left hand side.

$$-\left(1 + \mu\Delta\theta_k\right)F_k + F_{k-1} + B_f m_k g \left(\cos\left(\theta_k\right) + \mu\sin\left(\theta_k\right)\right) - m_k \frac{\partial^2 u_k}{\partial t^2} = 0$$

(46)

Define the displacement from the equilibrium position in each spring as x_k and the spring force

follows the Hooke's law. For this dynamic model, it is:

$$F_k = K_k x_k$$

(47)

The measurement depth of the component k is:

$$u_k = D\left(n - k\right) + \sum_{j=k}^{n-1} x_j - b$$

(48)

In Equation (48), downwards along the wellbore trajectory is the positive direction. The block

position b is defined as the negative value. Rotary Kelly Bushing (RKB) is the zero level. At the

initial moment, assume the springs are all at their own balanced positions, i.e. $x_j = 0$. u_k will be:

$$u_k = D\left(n - k\right) - b$$

(49)

According to the position change during tripping-out, i.e. the change of u_k, the Equation (50) can

estimate the acceleration. The second derivative of Equation (48) is:

$$\frac{\partial^2 u_k}{\partial t^2} = -\frac{\partial^2 b}{\partial t^2} + \sum_{j=k}^{n-1} \frac{\partial^2 x_j}{\partial t^2}$$ (50)

Substitute the Equation (50) into Equation (45) or Equation (46). In general, the resultant force will be:

$$-\left(1+\mu\Delta\theta_k\right)K_k x_k + K_{k-1}x_{k-1} + B_f m_k g\left(\cos\left(\theta_k\right) + \mu\sin\left(\theta_k\right)\right) - m_k\left(-\frac{\partial^2 b}{\partial t^2} + \sum_{j=k}^{n-1}\frac{\partial^2 x_j}{\partial t^2}\right) = 0$$ (51)

For the travelling block, i.e. the component n, the equation is:

$$-F_n + K_{n-1}x_{n-1} + B_f m_n g + m_n \frac{\partial^2 b}{\partial t^2} = 0$$ (52)

F_n is the simulated HKL. For the first component such as BHA, the equation is:

$$-\left(1+\mu\frac{\Delta\theta_1}{2}\right)K_1 x_1 + B_f m_1 g\left(\cos\left(\theta_1\right) + \mu\sin\left(\theta_1\right)\right) - m_1\left(-\frac{\partial^2 b}{\partial t^2} + \sum_{j=1}^{n-1}\frac{\partial^2 x_j}{\partial t^2}\right) = 0$$ (53)

Equation (51) to Equation (53) are a set of nonlinear ordinary differential equations. The equations use the travelling block position b and the initial displacement of the spring from the equilibrium position x_k as the inputs to solve the HKL F_n.

5.2.   Mathematical model applied in present thesis

The following two mathematical models are the fundaments of the simulation in present thesis. The first model is a static model. It can calculate the drag force at the static condition with the consideration of the side force, and then the static drag force can calculate the initial displacement in each section. The second model is designed for the dynamic simulation. This model utilizes the initial displacement calculated from the first model and utilizes the block position as the inputs to simulate the HKL. This model also considers the side force. Figure 15 is available to illustrate the following mathematical models.

5.2.1.   2D discrete static model

This model is a discrete model and has the ability to evaluate the influence of side forces when the drillpipe is forced to the ceiling of the wellbore. Based on force analysis in Figure 15, the forces can be decomposed along x and z direction. The red solid arrows indicate the x axis and

39

the z axis individually. Since this is a static analysis, the resultant forces along x and z direction are in balance.

The resultant force along x direction can be written as follows.

$$F_{xk} = B_f m_k g \cos(\theta_k) + \mu|N_k| - (F_k - F_{k-1})\cos\left(\frac{\Delta\theta_k}{2}\right) = 0 \tag{54}$$

The resultant force along z direction can be written as follows.

$$F_{zk} = -B_f m_k g \sin(\theta_k) + N_k + (F_k + F_{k-1})\sin\left(\frac{\Delta\theta_k}{2}\right) = 0 \tag{55}$$

Derive the normal force N_k from Equation (54):

$$N_k = \left| B_f m_k g \sin(\theta_k) - (F_k + F_{k-1})\sin\left(\frac{\Delta\theta_k}{2}\right) \right| \tag{56}$$

Substitute N_k into Equation (54). N_k has the absolute value sign and it contains the unknown term F_k which is what we are going to solve. Therefore, assume N_k to be positive first. The positive N_k means this part of the drillstring is attached at the lower side of the wellbore. Then Equation (54) becomes:

$$B_f m_k g \cos(\theta_k) + \mu\left(B_f m_k g \sin(\theta_k) - (F_k + F_{k-1})\sin\left(\frac{\Delta\theta_k}{2}\right) \right) - (F_k - F_{k-1})\cos\left(\frac{\Delta\theta_k}{2}\right) = 0 \tag{57}$$

Rearrange Equation (57)

$$B_f m_k g \left(\cos(\theta_k) + \mu\sin(\theta_k)\right) - F_k\left(\mu\sin\left(\frac{\Delta\theta_k}{2}\right) + \cos\left(\frac{\Delta\theta_k}{2}\right) \right) - F_{k-1}\left(\mu\sin\left(\frac{\Delta\theta_k}{2}\right) - \cos\left(\frac{\Delta\theta_k}{2}\right) \right) = 0 \tag{58}$$

Finally, derive an expression for F_k.

$$F_k = \frac{\left[B_f m_k g \left(\cos(\theta_k) + \mu\sin(\theta_k)\right) - F_{k-1}\left(\mu\sin\left(\frac{\Delta\theta_k}{2}\right) - \cos\left(\frac{\Delta\theta_k}{2}\right) \right) \right]}{\left(\mu\sin\left(\frac{\Delta\theta_k}{2}\right) + \cos\left(\frac{\Delta\theta_k}{2}\right) \right)} \tag{59}$$

For the deepest section, if the bit is off the bottom, then the drag force can be simplified as:

$$F_1 = \frac{B_f m_1 g \left(\cos(\theta_1) + \mu \sin(\theta_1)\right)}{\mu \sin\left(\dfrac{\Delta\theta_1}{2}\right) + \cos\left(\dfrac{\Delta\theta_1}{2}\right)} \tag{60}$$

Then assume the normal force N_k is negative, it means the drillstring is clinging to the ceiling of the wellbore. The resultant force, i.e. the side fore, is downward, and then the equation will be:

$$B_f m_k g \cos(\theta_k) - \mu\left(B_f m_k g \sin(\theta_k) - (F_k + F_{k-1})\sin\left(\frac{\Delta\theta_k}{2}\right)\right) - (F_k - F_{k-1})\cos\left(\frac{\Delta\theta_k}{2}\right) = 0 \tag{61}$$

Rearrange the above equation.

$$B_f m_k g \left(\cos(\theta_k) - \mu \sin(\theta_k)\right) + F_k \left(\begin{array}{c} \mu \sin\left(\dfrac{\Delta\theta_k}{2}\right) \\ -\cos\left(\dfrac{\Delta\theta_k}{2}\right) \end{array}\right) + F_{k-1}\left(\begin{array}{c} \mu \sin\left(\dfrac{\Delta\theta_k}{2}\right) \\ +\cos\left(\dfrac{\Delta\theta_k}{2}\right) \end{array}\right) = 0 \tag{62}$$

Finally, derive an expression for F_k.

$$F_k = \frac{\left[B_f m_k g \left(\cos(\theta_k) - \mu \sin(\theta_k)\right) + F_{k-1}\left(\mu \sin\left(\dfrac{\Delta\theta_k}{2}\right) + \cos\left(\dfrac{\Delta\theta_k}{2}\right)\right)\right]}{-\left(\mu \sin\left(\dfrac{\Delta\theta_k}{2}\right) - \cos\left(\dfrac{\Delta\theta_k}{2}\right)\right)} \tag{63}$$

For the lowest section at the end of the drillstring, if the bit is off the bottom, then the drag force can be simplified as:

$$F_1 = \frac{B_f m_1 g \left(\cos(\theta_1) - \mu \sin(\theta_1)\right)}{-\mu \sin\left(\dfrac{\Delta\theta_1}{2}\right) + \cos\left(\dfrac{\Delta\theta_1}{2}\right)} \tag{64}$$

So far, two drag forces for the same section are calculated, but only one should be included. During tripping-out, the resultant normal force will always generate friction no matter which side of the drillstring is attached to and the friction always resists the hook pulling out the drillstring. Therefore, the largest value of F_k should be the right one. The flow chart in Appendix B shows the detailed procedure.

5.2.2. Modified 2D dynamic model

Some challenges were discovered when programming the model in subchapter 5.1.7 with MATLAB. The following three points are the major challenges.

1. It is difficult to implement this model. The equation for each component contains different numbers of the acceleration term. The different numbers of the acceleration term in each equation require rearranging and solving the set of the equations in a specific order. In each time step, the equations solved have to be substituted into the equation being solved currently. The position of each component defined in Equation (48) is the sum of the spring displacement, the initial length of the components, and the BPOS. When calculating the second order derivative in Equation (50), it contains different numbers of the acceleration terms for a specific component. When the location of a specific component is very deep in the hole, Equation (50) will contain more acceleration terms than for the shallower components. In order to solve the unknown acceleration term, the equations should be solved from the top to the bottom. At the top component, it contains only one term of the acceleration. Substitute this solved acceleration term into the second top component, which then will contain two acceleration terms. Repeat this procedure for the rest of the components. Finally, all the acceleration terms can be solved. Theoretically, this method is feasible, but if the drillstring is divided into many components, the deepest component will contain many acceleration terms. It is difficult to solve with the high computation efficiency.

2. The model is difficult to converge, i.e. hard to provide good results. The simulation shows that the result is very different from the observed value on site.

3. The side force included in the previous model is improper. When the value of the normal force is positive such as when the drillstring is clinging to the upper side of the wellbore, this model can give the right answer. When the value of the normal force is negative such as the drillstring is clinging to the lower side of the wellbore, the model will give the improper result.

Aiming at solving the challenges in the original model, the following aspects are the improvements in this modified model.

1. Abandon the approximation in the original model, for example $\cos\left(\dfrac{\Delta\theta_k}{2}\right)\approx 1$ and

   $\sin\left(\dfrac{\Delta\theta_k}{2}\right)\approx\dfrac{\Delta\theta_k}{2}$. Because the mathematical model is solved by the computer, there is

   no necessity to make such an approximation, which will take errors into the modified

   model.

2. Define the acceleration term in a new way, which is easy to implement in the simulator.

   Same definition mentioned in Mass-spring model is applied. With this definition, every

   equation has only one acceleration term.

3. Redefine the meaning of x_k. x_k indicates the position of the lower end at each

   component. The first component is the BHA, so x_1 indicates the position of the lower end

   of BHA, i.e. the measured depth of the drill bit.

4. Add an absolute value sign beside the normal force. No matter if the drillstring is attached

   at the lower or the upper side in the wellbore, the friction is always acting downwards

   during the tripping-out.

5. Consider damping.

The following parts are the detailed derivation of this mathematical model.

We define the measured depth at the initial condition as $x_{kinitial}$ and the current position is x_k,
then the elastic force is defined as:

$$F_k = K_k\left(\left(x_k - x_{k+1}\right) - \left(x_k - x_{k+1}\right)_{initial}\right) \tag{65}$$

The first component is the deepest one, so $\left(x_k - x_{k+1}\right)$ should always be positive. For the last
component, the spring force is defined as:

$$F_n = K_n\left(\left(x_n + BPOS\right) - \left(x_n + BPOS\right)_{initial}\right) \tag{66}$$

For the first component, the spring force is defined as:

$$F_1 = K_1\left(\left(x_1 - x_2\right) - \left(x_1 - x_2\right)_{initial}\right) \tag{67}$$

No approximation is added in the derivation. For the first component such as the BHA:

$$B_f m_1 g \cos\theta_1 + \mu \left| B_f m_1 g \sin\theta_1 - F_1 \sin\left(\frac{\Delta\theta_1}{2}\right) \right| + F_1 \cos\left(\frac{\Delta\theta_1}{2}\right) - Dmpv = m_1 \frac{\partial^2 x_1}{\partial t^2} \tag{68}$$

Substitute the spring force in to Equation (68), the equation will then be:

$$B_f m_1 g \cos\theta_1 + \mu \left| B_f m_1 g \sin\theta_1 - K_1 \left[\begin{matrix} (x_1 - x_2) - \\ (x_1 - x_2)_{initial} \end{matrix} \right] \sin\left(\frac{\Delta\theta_1}{2}\right) \right| - K_1 \left(\begin{matrix} (x_1 - x_2) - \\ (x_1 - x_2)_{initial} \end{matrix} \right) \cos\left(\frac{\Delta\theta_1}{2}\right) - Dmpv = m_1 \frac{\partial^2 x_1}{\partial t^2} \tag{69}$$

Separate the acceleration term:

$$\frac{\partial^2 x_1}{\partial t^2} = \frac{1}{m_1} \left\{ B_f m_1 g \cos\theta_1 + \mu \left| B_f m_1 g \sin\theta_1 - K_1 \left[\begin{matrix} (x_1 - x_2) - \\ (x_1 - x_2)_{initial} \end{matrix} \right] \sin\left(\frac{\Delta\theta_1}{2}\right) \right| - K_1 \left(\begin{matrix} (x_1 - x_2) - \\ (x_1 - x_2)_{initial} \end{matrix} \right) \cos\left(\frac{\Delta\theta_1}{2}\right) - Dmpv \right\} \tag{70}$$

The general components, after separating the acceleration term, will become:

$$\frac{\partial^2 x_k}{\partial t^2} = \frac{1}{m_k} \left\{ \begin{matrix} B_f m_k g \cos\theta_k + \mu \left| \begin{matrix} B_f m_k g \sin\theta_k - K_k \left[\begin{matrix} (x_k - x_{k+1}) - \\ (x_k - x_{k+1})_{initial} \end{matrix} \right] \sin\left(\frac{\Delta\theta_k}{2}\right) \\ -K_{k-1} \left[\begin{matrix} (x_{k-1} - x_k) - \\ (x_{k-1} - x_k)_{initial} \end{matrix} \right] \sin\left(\frac{\Delta\theta_k}{2}\right) \end{matrix} \right| \\ -K_k \left(\begin{matrix} (x_k - x_{k+1}) - \\ (x_k - x_{k+1})_{initial} \end{matrix} \right) \cos\left(\frac{\Delta\theta_k}{2}\right) + K_{k-1} \left(\begin{matrix} (x_{k-1} - x_k) - \\ (x_{k-1} - x_k)_{initial} \end{matrix} \right) \cos\left(\frac{\Delta\theta_k}{2}\right) - Dmpv \end{matrix} \right\} \tag{71}$$

For the last component, i.e. the part of the drillstring near the wellhead, the equation is

$$\frac{\partial^2 x_n}{\partial t^2} = \frac{1}{m_n} \left\{ \begin{matrix} B_f m_n g \cos\theta_n + \mu \left| \begin{matrix} B_f m_n g \sin\theta_n - K_n \left[\begin{matrix} (x_n + BPOS) - \\ (x_n + BPOS)_{initial} \end{matrix} \right] \sin\left(\frac{\Delta\theta_n}{2}\right) \\ -K_{n-1} \left[\begin{matrix} (x_{n-1} - x_n) - \\ (x_{n-1} - x_n)_{initial} \end{matrix} \right] \sin\left(\frac{\Delta\theta_n}{2}\right) \end{matrix} \right| \\ -K_n \left(\begin{matrix} (x_n + BPOS) - \\ (x_n + BPOS)_{initial} \end{matrix} \right) \cos\left(\frac{\Delta\theta_n}{2}\right) + K_{n-1} \left(\begin{matrix} (x_{n-1} - x_n) - \\ (x_{n-1} - x_n)_{initial} \end{matrix} \right) \cos\left(\frac{\Delta\theta_n}{2}\right) - Dmpv \end{matrix} \right\} \tag{72}$$

Equations (71) and (72) are identical with each other, and contain the same terms. Equation (68) is derived only for the deepest component. Therefore, it will be easier to program with such a set of equations. If this set of equations contains many components, it will be quite convenient to program by means of a loop.

Above is the introductions of the mathematical models. We have reviewed all the models and their disadvantages and advantages. In the next chapter, the simulation result will be delivered to prove that this mathematical model is valid. A detailed input case for the simulator is manufactured based on the experimental design.

6. Simulation and result

The previous chapters introduced the experimental design and the mathematical models. Technically, to verify the correctness of the mathematical models, both the experiment and the simulation should be performed and be compared with each other. However, the experiment has not been set up yet due to technical challenges, but especially the time limitation. A feasible solution to validate the mathematical model is to manufacture fictive parameters, which are based on the experimental design, and then test the mathematical model with the manufactured inputs. If the model is valid, the simulated result should be reasonable, for example, at least the simulated result has a similar pattern as the observed result on site.

In Chapter 5.2, two mathematical models have been developed. The one is a static model and the other one is a dynamic model. In the first subchapter, the drag force will be calculated with the discrete static model developed in chapter 5.2.1 and the classical soft string model developed by B. Aadnoy and Andersen (1998). The results calculated from these two methods will be compared. In the second subchapter, the dynamic model will be tested against the manufactured inputs.

6.1.   Test of the discrete static model

A new mathematical model was developed to calculate the drag force in static condition. This model also considers the side force in the curved section. The classical soft string model developed by B. Aadnoy and Andersen (1998) will be used as the comparison.

The test case is based on Well C47. The detailed information about this well is introduced in Chapter 3.1. The drillstring tested in present subchapter is simplified by only using a uniform drillstring rather than an assembly of the different drill pipes. Table 4 shows the drillstring parameters, which will be tested in present subchapter.

The static drag forces at the two ends in each section are calculated with these two methods. Table 5 only shows the static drag force at the upper end of the buildup section and the normal force at this buildup section.

Table 4: Input drillstring parameters to be tested.

OD	ID	Weight		Cross section
inch	inch	ppf	kg/m	mm²
2-3/8	1.995	4.85	7.22	842
2-7/8	2.441	6.85	10.19	1169
3-1/2	2.992	9.50	14.14	1671
4	3.478	11.85	17.63	1984
4-1/2	3.958	13.75	20.46	2322

Table 5: Calculated static drag force and normal force with different models.

Type of drillpipe inch	Drag force at upper end in bended section			Normal force in bended section		
	Classic	Discrete	Error	Classic	Discrete	Error
	N	N	%	N	N	%
2-3/8	132340	123531	6.66	-90265	-85888	4.85
2-7/8	186780	174346	6.66	-127396	-121218	4.85
3-1/2	259182	241929	6.66	-176780	-168207	4.85
4	323153	301641	6.66	-220412	-209723	4.85
4-1/2	375026	350061	6.66	-255793	-243388	4.85

The classical method has been applied in industry for many years, and the calculation shows that the discrete model gives the similar result as the classical model. Therefore, the discrete model is also a valid model to calculate drag force during tripping operation. Two additional comments should be added here.

- The classic model requires identifying the well trajectory before applying the correct equation. Without the correct identification, it is not possible to utilize the classic model. The discrete method does not require identifying the well trajectory. The equation mentioned in the discrete model is a general model and can be applied in arbitrary sections. The discrete model avoids the error by choosing the improper equation in the classic method.
- The result in Table 5 considers the whole buildup section as one segment. However, the discrete model can be applied between any two arbitrary survey points. In this case, the buildup section contains 25 survey points. When applying the discrete method in these 24 segments rather than only one long segment, the model should deliver higher accuracy. The classic method is difficult to apply between any two survey points, especially two neighboring survey points, because the length is too short, and it is relatively difficult to identify the well trajectory type when the inclination and the azimuth change slowly.

6.2. Test of the 2D modified dynamic model

In present subchapter, the test case will be introduced first, and then the simulation result will be presented.

6.2.1. Test case

The test case is designed based on Chapter 3. BPOS is the important input in this dynamic model. The BPOS in this case is downscaled based on the real case. Some parameters such as the average velocity and the acceleration have been mentioned in Chapter 3.2. The block position used in this test can be defined in three stages.

1. Static stage. In this stage, the mass-spring chain is static. The BPOS will be at its initial position. The purpose of this stage is to let the system be still. This stage could last 10 to 15 seconds.

2. Acceleration stage. In this stage, the mass-spring chain accelerates with a constant acceleration. The velocity will increase from zero to a specific velocity. This stage lasts several seconds.

3. Constant velocity stage. In this stage, the mass-spring chain has finished the acceleration. The velocity is now constant.

Figure 16 shows the detailed information about the block position applied in this case.

BPOS vs. Time
Initial velocity: 0 m/s   Acceleration time: 3 s
Acceleration: 0.001 m/s2   Average velocity: 0.003 m/s
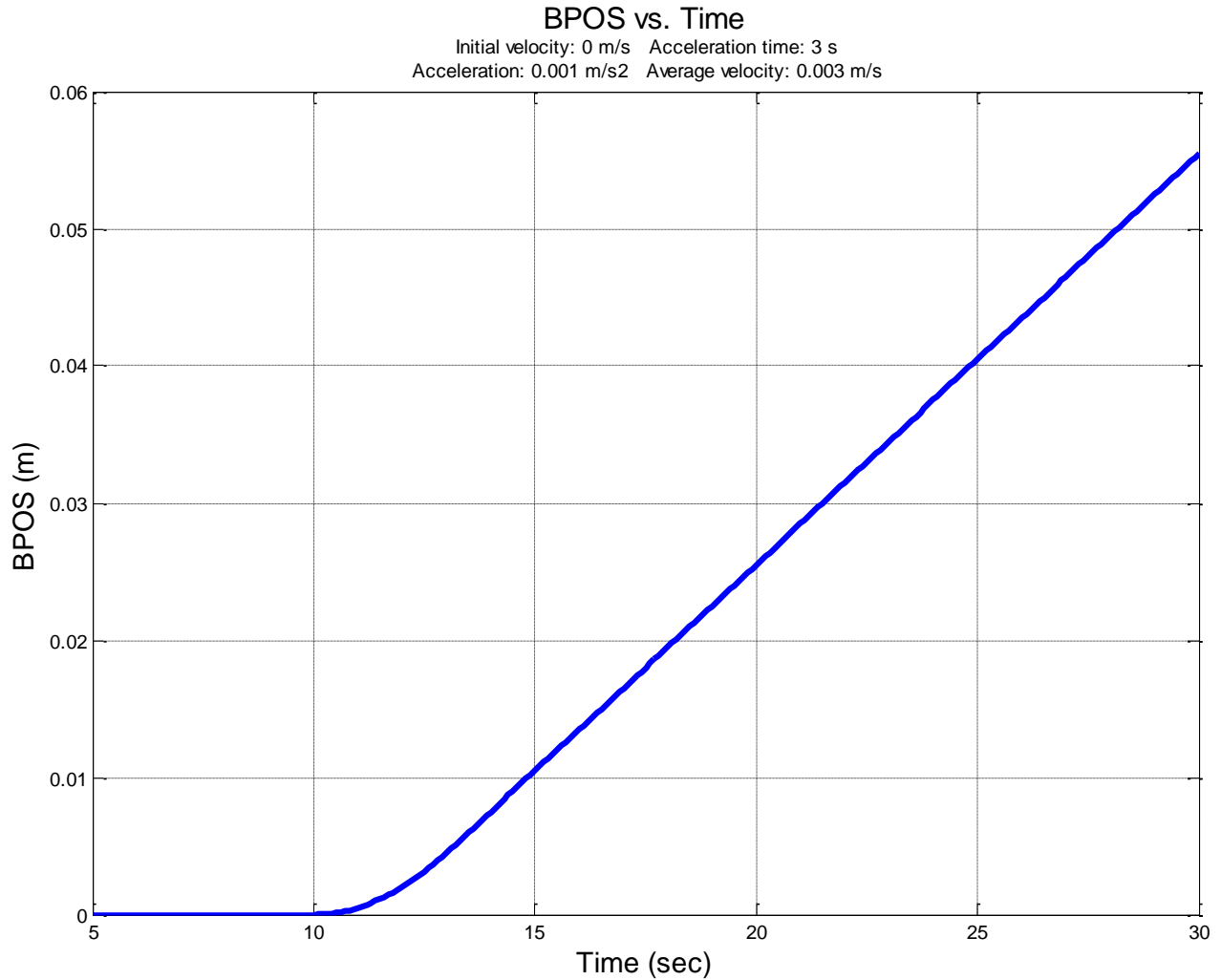
Figure 16: BPOS vs. time applied in the test.

What kind of mass-spring chain applied in the experiment is another issue. A simple mass-spring chain can be like this:

- Four mass blocks linked together with four springs.

- The lowest mass block is a huge block representing the drillpipe below the buildup section. The remaining three mass blocks consist of a 2-7/8 inch drillpipe cut into three pieces.

- A spring (wireline) connects the upper end of this chain and the winch. Another spring (wireline) connects the huge block and the lower end of this chain to the curved pipe. The next two normal springs connect three neighboring mass blocks to the buildup section.

If the total length of this chain is constant and consists smaller pieces of mass blocks, then the springs will lead to more accurate simulation result. It also indicates that the simulation will be more time-consuming. To validate this dynamic model, the mass-spring chain does not have to be too complex. Table 6 presents the detailed information about this chain.

Table 6: Detailed information about this chain.

Mass blocks	Length meter	Weight kg	Springs	Length meter	Elasticity N/m
1-lowest	-	2000	1-wireline	5	277310
2-in buildup	2.36	20.38	2-normal spring	0.48	4151
3-in buildup	2.36	20.38	3-normal spring	0.48	4151
4-in buildup	2.36	20.38	4-wireline	5	277310

With the determined mass-spring chain, the well trajectory data at each mass block can be determined. Based on the survey data, Table 7 shows the inclination change and the average inclination at each mass block.

Table 7: Survey data at each mass block.

Mass block	incl_average rad	incl_change rad
1-lowest	1.57	0.00
2-in buildup	1.32	0.25
3-in buildup	0.84	0.22
4-in buildup	0.31	0.31

Except for the parameters mentioned above, other information shown in Table 8 are necessary. Now the mathematical model can be validated.

Table 8: Other parameters as inputs.

damping Ns/m	buoyancy factor	Friction coefficient	Gravity m/s²
300	0.79	0.25	9.81

6.2.2. Test result

The simulation result will be presented based on the above case. Figure 17 shows the simulated HKL. This curve is similar to the observed result in the real case presented by Xie (2014). It must be stated here that the string is in neutral tension only due to gravity. The friction due to tripping-in or out has been neutralized (through drillstring rotation for instance). The HKL indicates the static drag force in the first ten seconds. The next three seconds is the acceleration stage; the simulated HKL increases linearly since the acceleration is a constant. The last stage is the constant velocity stage. The initial HKL peak can be observed at the beginning of this stage. In the real case, this initial peak also exists. Depending on the specific downhole situation, the value of the initial peak could be even larger.

Figure 18 shows the displacement at each section. During tripping-out, the drillstring is not influenced by historical friction in the axial direction. From this figure, it can be observed that the deepest mass block (section 1) moves only $31.56\,mm$, and the shallowest mass block (section 4) moves $55.09\,mm$. The BPOS shows that the maximum travelling distance is $55.50\,mm$. The simulation shows that the drillstring is extended during the tripping-out operation. A brief explanation will be mentioned in Chapter 7.3.
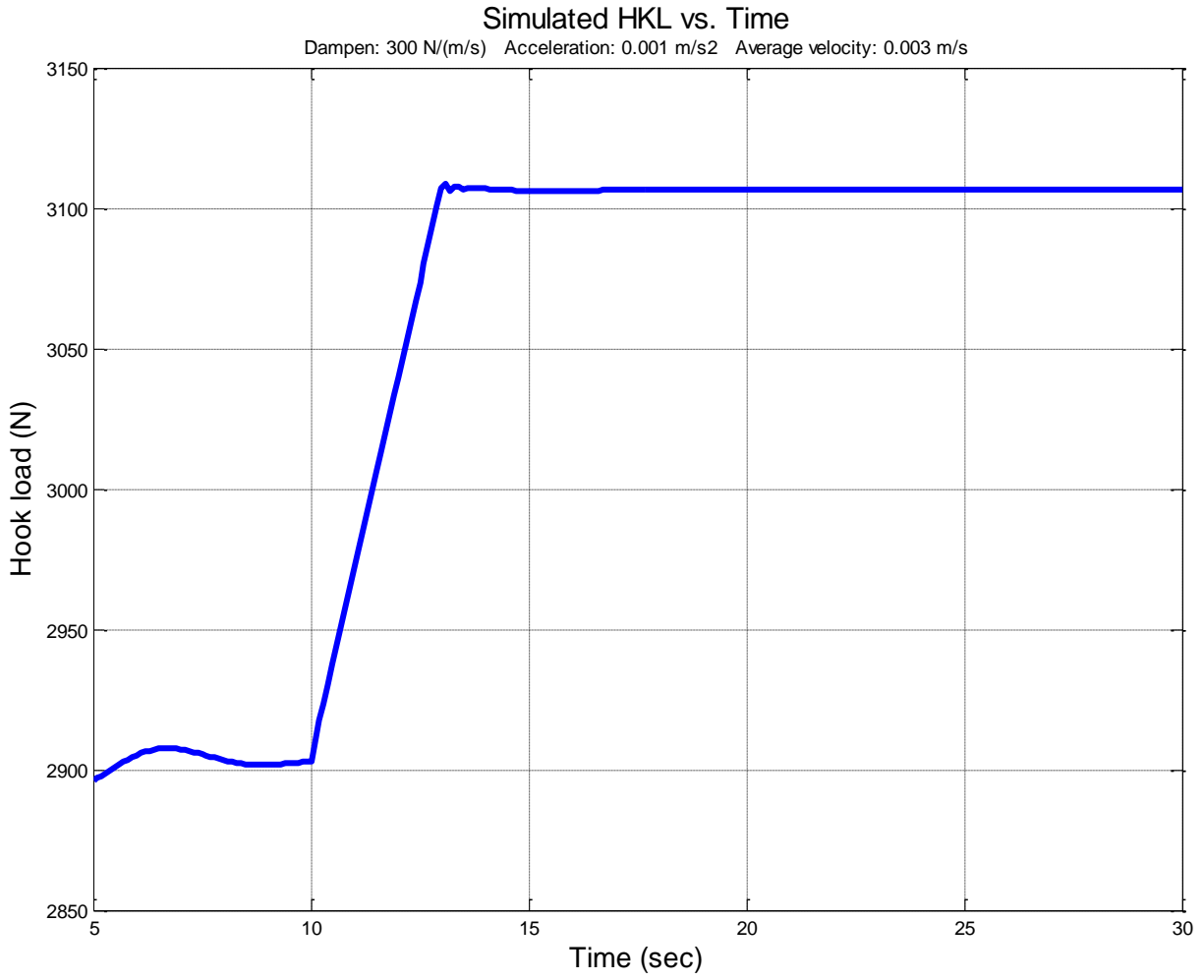
Figure 17: Simulated HKL vs. time.
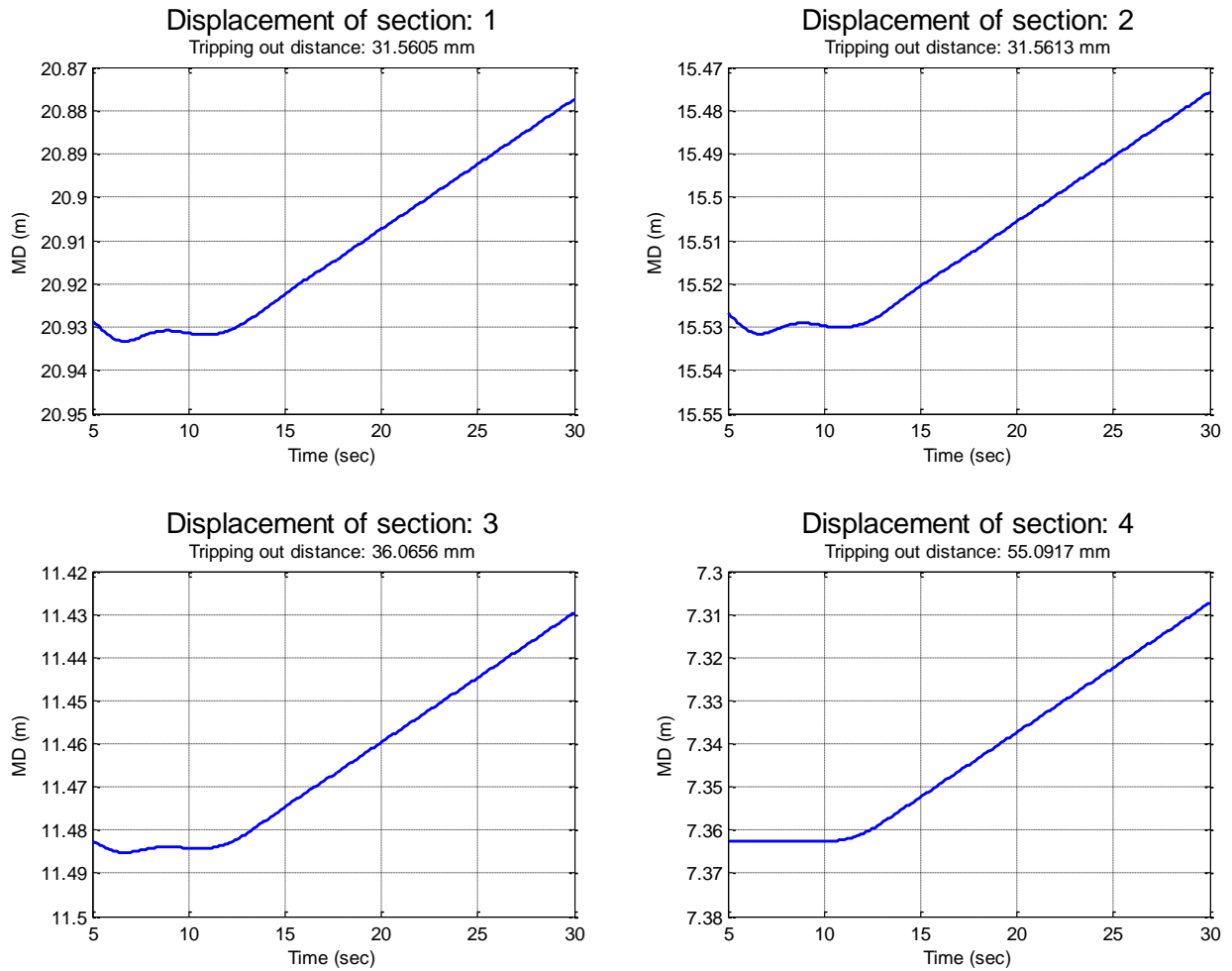
Figure 18: Displacement for each section after pulling the string 55.5 mm.

Figure 17 and Figure 18 are the main output of this dynamic mathematical model. Meanwhile, Figure 19 and Figure 20 give a close observation at one time interval, and will be helpful to understand what happens in each time interval. In this case, the time interval is $0.1\,s$. These two figures show that all the sections behave normally except section 4. The velocity and acceleration in section 4 indicate that this section vibrates severely. This observation will be discussed in Chapter 7.4.
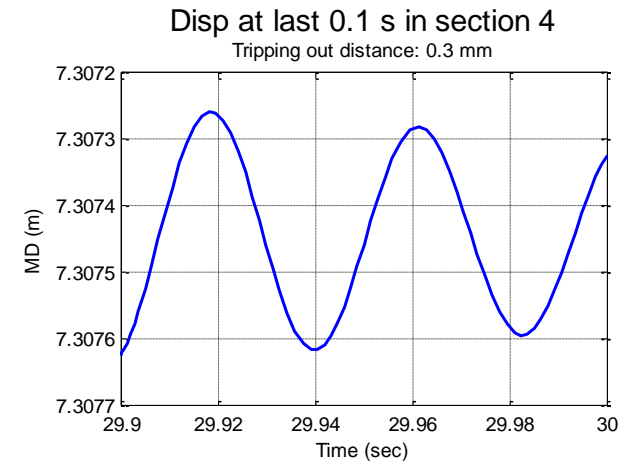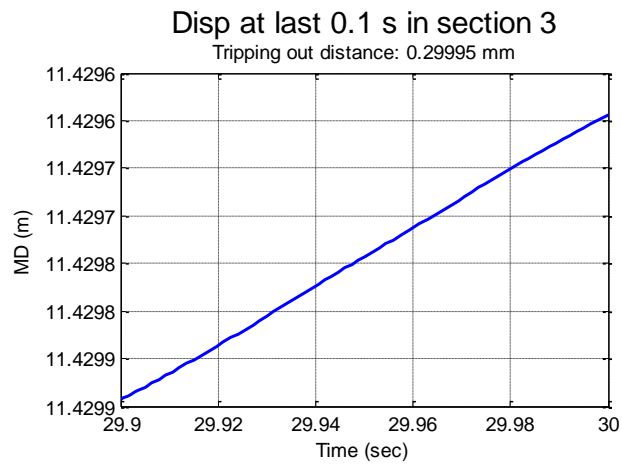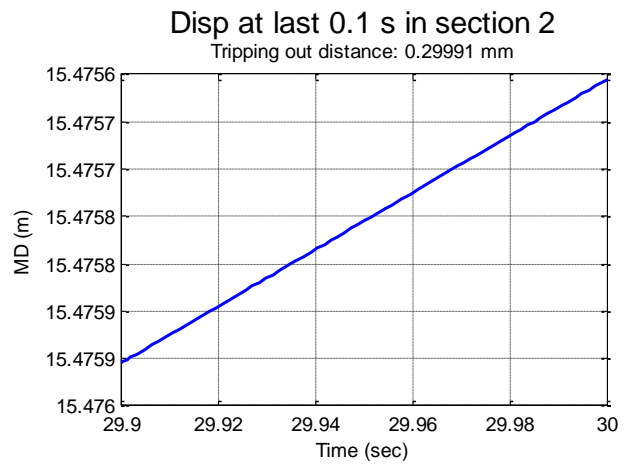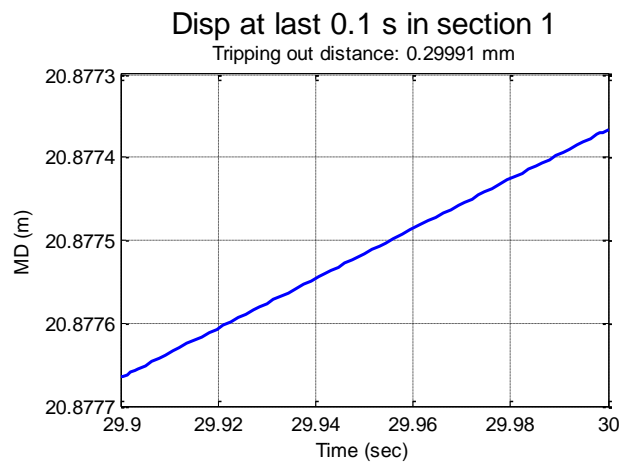
Figure 19: Displacement in each section at one time interval.
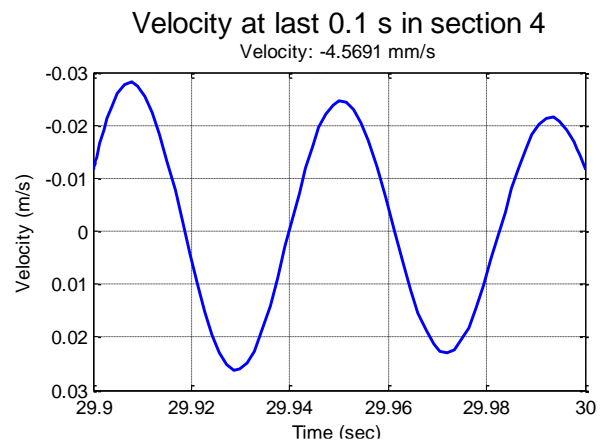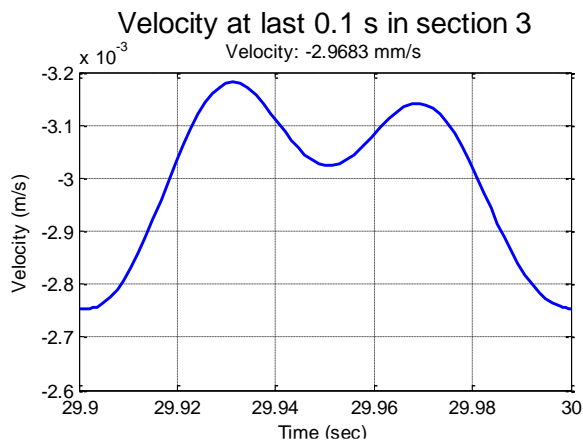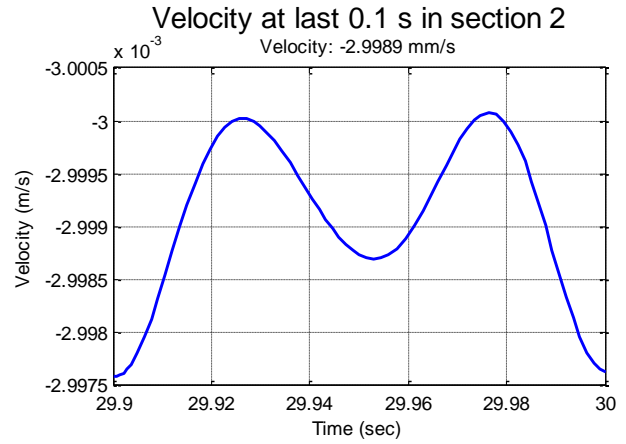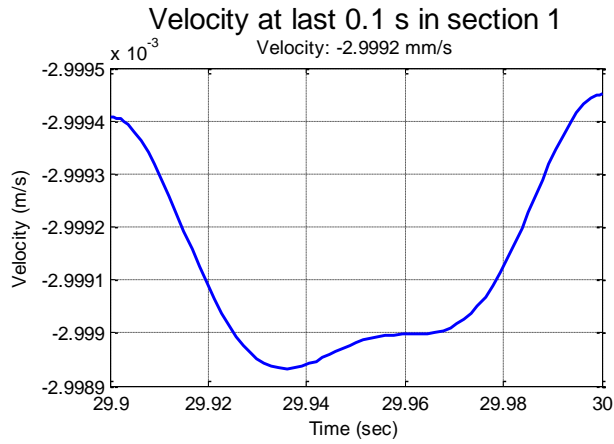
Figure 20: Velocity in each section at one time interval at four different temporal spots.

Above all this is the simulation result for the two models introduced in Chapter 5.2. In Chapter 7, some issues about the experimental design and the mathematical model will be discussed.

7. Technical Discussion

In previous chapters, the experimental design, the mathematical models, and the simulation results were introduced. Several technical issues about the previous content will be discussed here.

7.1. Is downscaling calculation a compulsory step or not?

In Chapter 3.2 Experimental design, the downscaling calculation was presented. The purpose of the downscaling calculation was to downsize the real well trajectory to the lab scale, so the proper components could be chosen and installed in the workshop. The downscaling calculation was indeed helpful for the experimental design. However, this step cannot be compulsory for these two reasons:

1. The purpose of the experiment was to repeat what happens on site, and to verify the correctness of the mathematical models. The mathematical models applied in present thesis were two general models, which can calculate the HKL under static and dynamic situations, separately. A well-developed general mathematical model should have the ability to simulate any specific cases. Therefore, the experiment did not have to follow the real case strictly. In this research, the experimental design was based on a specific real case. If the mathematical model was correct, the simulation should follow the experimental result for this specific well.

2. Even if the experiments were designed to follow a real specific case, in the process of assembling in the workshop, some limitations prevented assembling the setup exactly as the design in the setup draft predicted. For example, when manufacturing the curved pipe with the bending machine, it is difficult to create exactly the same inclination as calculated based on the survey data. After machine bending, the new inclination should be measured again and then the inclination should be updated in the simulator.

7.2. Application of the friction models and the effect of the contact surface

The friction models and the effect of contact surface were introduced in Chapter 4, but not all of these friction models have been applied in the simulation. Currently, the mathematical model applied in the simulation only considered the classic Coulomb friction model due to two reasons:

1. In present thesis, the most important task about the simulation was to validate the models. This aim was reached so far. According to the simulation by Xie (2014), the friction model indeed influenced the curve of the HKL, but the magnitude of the HKL was not influenced much. An interface for different friction models can easily be set up based on the current MATLAB code. Different friction models can be tested in future research on basis of the experimental results.

2. These friction models could be tested in present thesis, but no experimental results was available for comparing with the simulation result to verify which friction model would fit the experiment best. Therefore, testing with different friction models can be delivered in future research after the experimental result has been obtained.

7.3. Explanation about the drillstring elongation

The simulation result is Chapter 6.2.2 shows that the drillstring was extended during tripping-out. A brief explanation is given about this phenomenon.

At the initial moment of tripping-out, upward movement of the mass-spring chain led to elastic tension increase. The additional elastic force led to additional normal force, because the direction of the elastic force F_k was not collinear with the x direction in the buildup section shown in Figure 15. The additional normal force led to axial friction increase based on the Coulomb friction model. The additional axial friction led to elastic force increase during tripping-out. Based on Hook's Law, the drillstring was elongated. Now a loop feedback is formed, until the drillstring reaches an equilibrium state such as tripping-out at constant velocity.

If the explanation follows what happens on site, it indicates that the mathematical model is valid. The next step is to set up the experiment and verify the mathematical model based on the experimental result.

7.4. Explanation about the vibration in section 4

Figure 19 and Figure 20 showed that the displacement curve and the velocity curve vibrate severely at one time spot in section 4. With the literature investigation and the simulations with different inputs, damping is the most likely reason behind the vibration.

During tripping-out, the friction between the wellbore and the drillstring will transfer kinetic energy into thermal energy, so the drillstring vibration will finally stop. Kamel and Yigit (2014) presented a reasonable damping level in their study case, which is around $20000 \ Ns/m$ for a real case. Since the magnitude of the drag force was decreased in the experiment, damping should also decrease. The damping applied in Chapter 6.2.2 was $300 \ Ns/m$ for every section. The severe vibration indicates that the damping was too small. A case with $5000 \ Ns/m$ damping in section 4 was tested. The result in Figure 21 shows that section 4 still vibrates during tripping-out, but with less magnitude.
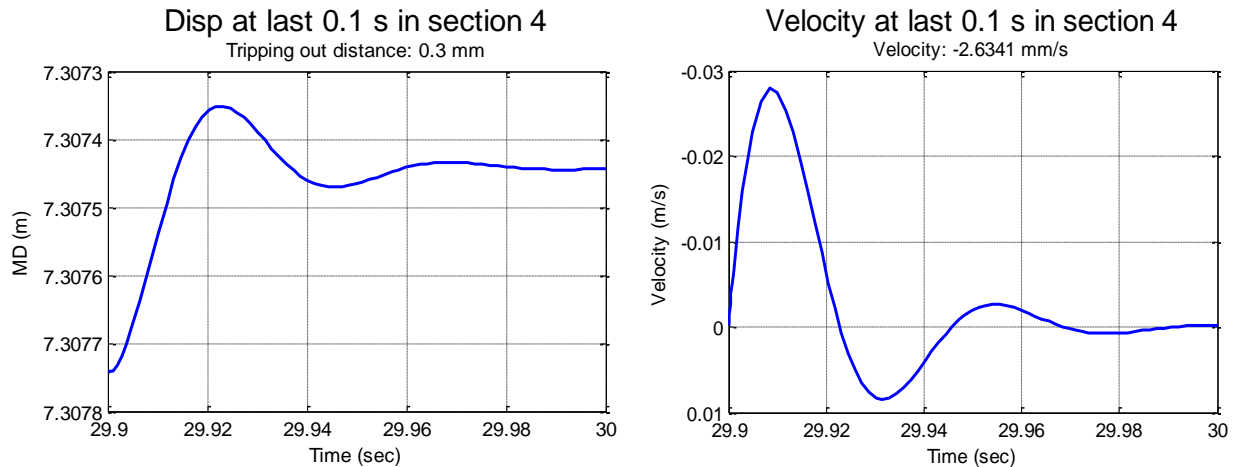
Figure 21: Displacement and velocity in section 4 with 5000 Ns/m of damping.

8. Self-evaluation

This chapter will analyze the possible sources of poor quality in the experimental part and in the simulation. Some suggestions for the future work will consider these issues.

8.1.   Sources of poor quality in the experiments

The experiments are not always as accurate as we think. The defect of the equipment, the limitation of the installation, and the data collection during the test often lead to deviation from reality in the experiment. Some possible reasons are mentioned here.

1. Defects in the equipment

In the experimental design, all the equipment are regarded as perfect products. For example, the equipment can run like what the designer wants. In reality, the equipment often have defects more or less during the process of manufacture. These defects will induce errors in the experiment.

- A bending machine will manufactured the curved pipe mentioned in Chapter 3.3. If the bending machine used to manufacture this curved pipe does not have enough accuracy, the curvature of the pipe will deflect from the initially designed curvature. This deflection will bring errors in the experiment if no proper rectification is performed.

- The motor should have the ability to control the output power precisely. Figure 16 indicates that the motor should be able to generate a BPOS with slow and smooth acceleration and velocity. BPOS is the most important input in the experiment and the simulation. If the motor-generated BPOS is not smooth enough or the BPOS changes abruptly, the results will be severely influenced.

- In the experimental design, no friction is considered in the pulley system. In reality, when the wireline with high drag force travels through the pulley system and the pulley system changes the direction of the wireline, the HKL could take additional friction into the experiment. This additional friction cannot be measured specifically in the experiment. The additional friction in the pulley system is also not considered in the mathematical

model. It might cause the simulation result and the experimental result not to be consistent with each other.

- Two scaffolds are used to support the curved pipe and the huge mass block separately. Especially during tripping-out, the friction will cause the equipment to vibrate, and then influence the data collection if the vibration is severe. Based on this consideration, a sufficiently strong scaffold should be applied.

2. *Limitation in the process of the installation*

Even through the equipment has been downsized based on the downscaling calculation, the whole setup is still very large in lab scale. For example, the curved pipe is 10-meter long. To assemble such a big pipe on the scaffold, proper tools are needed. Two issues should be considered in this process.

- The purpose of the experiment is to verify the 2D mathematical model, so the curved pipe should be installed vertically, i.e. without azimuth change. In the case of azimuth change, the simulation result will not be consistent with the experimental result, since the 2D mathematical model cannot simulate the scenario with azimuth change.

- How to fix the curved pipe on the scaffold is another issue. The curved pipe and the scaffold can be fixed together by welding. The welding can fix the pipe firmly on the scaffold, but will prevent replacing the curved pipe easily when another experiment with different curved pipe should be required in future research. Pipe fastener is another method to fix the curved pipe and the scaffold. This method is convenient to operate but untight fastener will induce additional vibration during the test, which may take errors into the experiment.

3. *Data collection during the test*

The velocity gauge and the load cell should have enough sensitivity and should not be influenced by other electrical equipment. Sjøberg (2014) mentioned when the winch was running, the noise could be observed in the data collected by the load cell. The winch generated electrical pulses when running. If pulses were observed in the data, some counter measurements had to be taken,

such as grounding the electrical equipment. Filters can also be applied in the LabVIEW to reduce noise.

8.2. Sources of errors in the simulation

Generally, the error of the simulation have to be analyzed when the numerical method is applied to evaluate the mathematical model. Some possible sources of errors in the simulation are mentioned here.

1. *Improper friction model*

The friction model applied in the simulator was the Coulomb friction model. Based on the discussion in Chapter 4.1.1, the friction behavior may not follow the Coulomb friction model in wellbores while circulating. Therefore, when applying the Coulomb friction model the simulation result could contain error caused by improper friction model.

Even if the Coulomb friction model is proper both in the simulation and in the experiment, how to determine the Coulomb friction coefficient is an important issue. This coefficient has to be determined by the specific experiment or tests.

2. *Improper dampening*

Dampening is another parameter which has to be determined experimentally or based on the on-site observation. Just like the friction coefficient, improper dampening will induce errors in the simulation.

3. *Influence of the section length*

The static model and the dynamic model are both discrete models. Compared with the analytical model, the discrete model is born with errors. To apply the discrete model, the drillstring has to be discretized into small sections. In Chapter 6, the mass-spring chain was discretized into four sections. The simulation would therefore be influenced with relatively big error. If the mass-spring chain can be discretized into more sections, the simulation result will be closer to the analytical result and the error will be smaller. The downside is that more time is required with more sections.

4. Inaccurate inputs

The inputs of the simulation is based on measurements from real experiments. During measuring, the errors will be created even with correct operations. It is called system error. System error cannot be avoided since it is the feature of the measuring apparatus. For example, the minimum scale of the ruler is centimeter, it is not possible to measure millimeter with this ruler. System errors will also influence the simulation. What the researcher can do is to avoid accidental errors by calibrating the measurement.

8.3.   Potential improvements for the future work

There are still a lot of work to do on this topic. Some interesting areas are listed here.

1. 3D mathematical models

Azimuth is another important parameter in the survey data. Azimuth change will also create side forces and thus influence the HKL. The static and dynamic models developed in present thesis are 2D models. In future research, 3D static and dynamic models should be developed. At that time, experiments for 3D scenario should be delivered by testing the HKL with azimuthal change.

2. Consideration of the drillpipe stiffness

Currently, the mathematical models applied in present thesis are all based on the soft string model, i.e. the stiffness of the drillstring will not contribute to the side force. In Chapter 4.2.2, a model to calculate the side force was developed with the consideration of pipe stiffness. Side forces can be included in future simulation when high stiffness pipes are applied in the experiment.

3. Solve the dynamic mathematical model with different methods

In present research, the dynamic mathematical model is a set of ODEs. Runge-Kutta method is applied to solve this kind of mathematical model, which is a widely applied iterative method with high accuracy in a single step calculation. When the model contains more equations, i.e. more sections, the Runge-Kutta method is still available but with higher time consumption. Other methods can be tried to solve this mathematical model such as the finite differential method or the finite element method.

4. Test more scenarios in the experiment

The experiment to be performed in the next step is tripping-out operation through a 2D curved pipe. Since the experimental design in present thesis also considers even more scenarios, more cases can be tested in future research:

- Test tripping-out HKL with azimuth change.
- Test tripping-out HKL with circulation.
- Test tripping-out HKL with the issue of cutting transportation.
- Combination of the above three scenarios.

9. Conclusion

Both the experiment, the mathematical model and the simulation will be developed continuously in future research. Currently, we can deliver the following conclusions.

1. Based on downscaling calculations for Well C47, the experiment is designed with a setup draft. Currently, the experiment considers the influence of side forces in the buildup section. The setup also has the potential to support future research.

2. Mechanisms of side forces are analyzed based on both the soft string and the stiff string model. An equation to calculate side forces is derived based on the bending force of a beam.

3. A 2D static discrete mathematical model is derived. This model can calculate static drag forces considering side forces. This model can be applied on any well trajectory by means of only one general equation. The case study shows that this model is as accurate as the classic soft string model.

4. A 2D dynamic discrete mathematical model is developed based on previous work. This model considers side forces in the buildup section. An artificial case study shows that the simulation provides reasonable results, thus proving that this model is valid. Experiments are required to verify the correctness of this model in future research.

Nomenclature

Abbreviations

BHA   Bottom Hole Assembly
BPOS   Block Position
DOF   Degree of Freedom
HKL   Hook Load
MD   Measured Depth
NPT   Non-Productive Time
ODE   Ordinary Differential Equations
RTDD   Real Time Drilling Data
WOB   Weight on Bit.

Parameters

A	Amplitude	–
A_{cs}	Area of material cross section	mm^2
B	Buoyancy factor	–
C_s	Correction factor	–
D	Distance between the centers of cylinders (mass components)	m
Dmp	Damping	Ns/m
E	Young's model	MPa
F	Static friction or friction	N
F'	Dynamic friction	N
F_{break}	Breakaway friction or maximum static friction force	N
F_c	Coulomb friction	N
F_D	Fluid drag force or drag force	N
$F_{D,BHAn}^{\ t}$	Fluidic drag force for BHA at time t	N
F_{Dn}	Fluidic drag force for the mass n	N
$F_{Dn}^{\ t}$	Fluidic drag force for general mass n at time t	N
F_N	Normal force applied on the interface	N
$F_{fn}^{\ t}$	Friction force for mass n at time t	N
F_{fn}	Frictional force for the mass n	N
F_k	Spring force	N
F_n	Normal force along the radial direction	N
$F_{spring}^{\ t}$	Total spring force at time t	N
F_{smooth}	Smooth friction force	N
F_{stoc}	Stochastic friction force	N

F_t	Drag force at the lower end	N
$F_{t+\Delta t}$	Drag force at the upper end	N
F_{weight}	Drillstring weight considering buoyancy at time t	N
HKL^t	HKL at time t during tripping out	N
K_G	Geometric stiffness	N/m
L	Length for each section	m
$L_{element}$	Length of component	m
L_{string}	Drill string length	m
N	Normal force resultant	N
O	Gravity force along z direction	N
P	Gravity force along x direction	N
Q	Resultant friction caused by normal force resultant	N
S	General stochastic friction function	$-$
W	Drillstring weight submerged in mud	N
W_V	The vertical projected buoyant weight of pipe	N
a_n	Acceleration of drillstring at mass n	m/s^2
b	Position of travelling block	m
c_v	Reverse of sliding speed coefficient	s/m
d_h	Diameter of borehole	in
d_s	Diameter of drillstring	in
f	Static friction coefficient	$-$
f'	Dynamic friction coefficient	$-$
frq	Frequency	Hz
g	Gravity	m/s^2
k	Elasticity coefficient	N/m
$k_{(n-1)n}$	Elasticity coefficient between mass $n-1$ and n	N/m
k_{sat}	Constant coefficient to determine Coulomb and viscous friction model	kg/s
k_v	Friction coefficient	$-$
m	Linear mass for each section	kg
q_{pump}	Volume flow rate defined by the pump	m^3/s
u_k	Measure depth for the component k	m
v	Relative velocity between drillstring and drilling fluid	m/s
v_{ds}	Speed of tripping out	m/s
v_{mud}	Fluid velocity in the annulus	m/s
w_{unit}	Linear density of the drillstring	kg/m
w_N	Unit buoyant weight projection on the normal direction	kg/m
x	Elongated part of the drill string due to the HKL increase	m

x_k	Displacement from equilibrium position in the spring	m
x_n	Position of the drillstring at mass n	m
ΔL	Deformation along the force direction	m
$\Delta_{(n-1)n}$	Initial distance between elements $n-1$ and n	m
$\Delta\alpha$	Azimuth change	$\circ$
$\Delta\theta$	Inclination change	$\circ$
α	Azimuth	$\circ$
ε	Strain	$-$
θ	Inclination at mass n	$\circ$
$\bar{\theta}$	Average inclination of the component	$\circ$
λ	Elastic modulus	MPa
μ	Friction factor, not indicated it is dynamic or static	$-$
ρ	density of drilling mud and steel	kg/m^3
σ	Stress	MPa
τ	Shear stress at the surface of pipe	MPa

Reference

1. Aadnoy, B., & Andersen, K. (1998). *Friction analysis for long-reach wells.* Paper presented at the IADC/SPE drilling conference.

2. Aadnøy, B. S., & Andersen, K. (2001). Design of oil wells using analytical friction models. *Journal of petroleum Science and Engineering, 32*(1), 53-71.

3. Aadnoy, B. S., Fazaelizadeh, M., & Hareland, G. (2010). A 3D analytical model for wellbore friction. *Journal of Canadian Petroleum Technology, 49*(10), 25-36.

4. Andersson, S., Söderberg, A., & Björklund, S. (2007). Friction models for sliding dry, boundary and mixed lubricated contacts. *Tribology international, 40*(4), 580-587.

5. Bjerke, H. (2013). Revealing Causes of Restrictions by Signatures in Real-Time Hook Load Signals.

6. Cayeux, E., & Daireaux, B. (2009). *Early Detection of Drilling Conditions Deterioration Using Real-Time Calibration of Computer Models: Field Example from North Sea Drilling Operations*. Paper presented at the SPE/IADC Drilling Conference and Exhibition.

7. Cayeux, E., Daireaux, B., Dvergsnes, E., & Saelevik, G. (2012a). Early symptom detection on the basis of real-time evaluation of downhole conditions: Principles and results from several north sea drilling operations. *SPE Drilling & Completion, 27*(04), 546-558.

8. Cayeux, E., Daireaux, B., Dvergsnes, E. W., Saelevik, G., & Zidan, M. (2012b). *An Early Warning System for Identifying Drilling Problems: An Example From a Problematic Drill-Out Cement Operation in the North-Sea.* Paper presented at the IADC/SPE Drilling Conference and Exhibition.

9. Christophersen, L., Gjerde, J., & Valdem, S. (2007). *Final Well Report - Drilling and Completion 34/10-C-47*. Retrieved from Stavanger:

10. Cordoso Jr, J. V., Maidla, E. E., & Idagawa, L. (1995). Problem Detection During Tripping Operations in Horizontal and Directional Wells. *SPE Drilling & Completion, 10*(02), 77-83.

11. Falconer, I., Belaskie, J., & Variava, F. (1989). *Applications of a Real Time Wellbore Friction Analysis.* Paper presented at the SPE/IADC Drilling Conference.

12. Fazaelizadeh, M., Hareland, G., & Aadnoy, B. (2010). Application of New 3-D Analytical Model for Directional Wellbore Friction. *Modern Applied Science, 4*(2), p2.

13. Glomstad, T. S. (2012). *Analysis of Hook load Signal to reveal the Causes of Restrictions.* (MSc), NTNU, Trondheim, Norway.

14. Hibbeler, R. (2010). Mechanics of Materials-8th: Prentice Hall, Upper Saddle River.

15. Ho, H. (1988). *An improved modeling program for computing the torque and drag in directional and deep wells.* Paper presented at the SPE Annual Technical Conference and Exhibition.

16. Johancsik, C., Friesen, D., & Dawson, R. (1984). Torque and drag in directional wells—prediction and measurement. *Journal of Petroleum Technology, 36*(7), 987-992.

17. Kamel, J. M., & Yigit, A. S. (2014). Modeling and analysis of stick-slip and bit bounce in oil well drillstrings equipped with drag bits. *Journal of Sound and Vibration, 333*(25), 6885-6899.

18. Kristensen, E. (2013). *Model of Hook Load During Tripping Operation.* (MSc), NTNU, Trondheim, Norway.

19. Larsen, C. M. (2015). Marine Riser Analysis-an incomplete and preliminary collection of lecture notes and papers. 8.

20. Maidla, E. E. (1987). *Borehole friction assessment and application to oil field casing design in directional wells.* Louisiana State Univ. and Agricultural and Mechanical Coll., Baton Rouge, LA (USA).

21. Maidla, E. E., & Wojtanowicz, A. K. (1990). Laboratory study of borehole friction factor with a dynamic-filtration apparatus. *SPE Drilling Engineering, 5*(03), 247-255.

22. Mason, C., & Chen, D. C. (2007). *Step changes needed to modernise T&D software.* Paper presented at the SPE/IADC Drilling Conference.

23. MathWorks. (2015). Translational Friction. *Friction in contact between moving bodies.* Retrieved from http://se.mathworks.com/help/physmod/simscape/ref/translationalfriction.html

24. McSpadden, A., Brown, P., & Davis, T. (2001). *Field Validation of 3-Dimensional Drag Model for Tractor and Cable-Conveyed Well Intervention.* Paper presented at the SPE Annual Technical Conference and Exhibition.

25. Mitchell, R. F., Bjorset, A., & Grindhaug, G. (2015). Drillstring Analysis With a Discrete Torque/Drag Model. *SPE Drilling & Completion, 30*(01), 5-16.

26. Mitchell, R. F., & Samuel, R. (2009). How good is the torque/drag model? *SPE Drilling & Completion, 24*(01), 62-71.

27. Mme, U., Skalle, P., Johansen, S., & Sangesland, S. (2012). *Analysis and modeling of normal hook load response during tripping operations*. Retrieved from Trondheim:

28. Polak, M. A., & Lasheen, A. (2001). Mechanical modelling for pipes in horizontal directional drilling. *Tunnelling and underground space technology, 16*, 47-55.

29. Quigley, M., Dzialowski, A., & Zamora, M. (1990). *A Full-Scale Wellbore Friction Simulator.* Paper presented at the SPE/IADC Drilling Conference.

30. Sangesland, S. (2012). *Analytical model vJDA, rev. 2.2012 Force in curved horehole analysis (bend)*

31. Sjøberg, A. S. (2014). *Building, Testing and Qualifying New Hook Load Rig.* (Master of Science), NTNU, Trondheim, Norway.

32. Stribeck, R. (1903). Die wesentliche Eigenschaften der Gleit-und Rollenlager. Z. VDI 46 (1902). *VDI-Forschungsheft, 7*.

33. Swahn, I., Johansen, S. T., Hovda, S., & Skalle, P. (2014). *Detection of Abnormal Hook Load Response During Tripping Operations (work in progress)*.

34. Well Integrity Inspection. (2015). Retrieved from https://www.youtube.com/watch?v=bYjFy3z4OU0

35. Wikipedia. (2015, 13 April 2015). Sign function. Retrieved from https://en.wikipedia.org/wiki/Sign_function

36. Wu, A., Hareland, G., & Fazaelizadeh, M. (2011). Torque & drag analysis using finite element method. *Modern Applied Science, 5*(6), p13.

37. Xie, X. (2014). *Semester Project: Acceleration of the drill string in the lab, in the field and theoretically.* (non-degree), NTNU, Trondheim, Norway.

Appendix

A. Setup draft

Setup Draft

Legend:
1. Curved pipe
2. Transition pipe
3. Horizontal pipe
4. Mass-spring chain
5. Pulley system
6. Velocity gauge
7. Load cell
8. pulley on surface
9. Wireline
10. Fluid piping
11. Mass block
12. Flowmeter
13. Separator
14. Mud tank
15. Cutting tank
16. Mud pump
17. Winch & Motor
18. Scaffold-pipe
19. Scaffold-block
20. Pipe T & seal
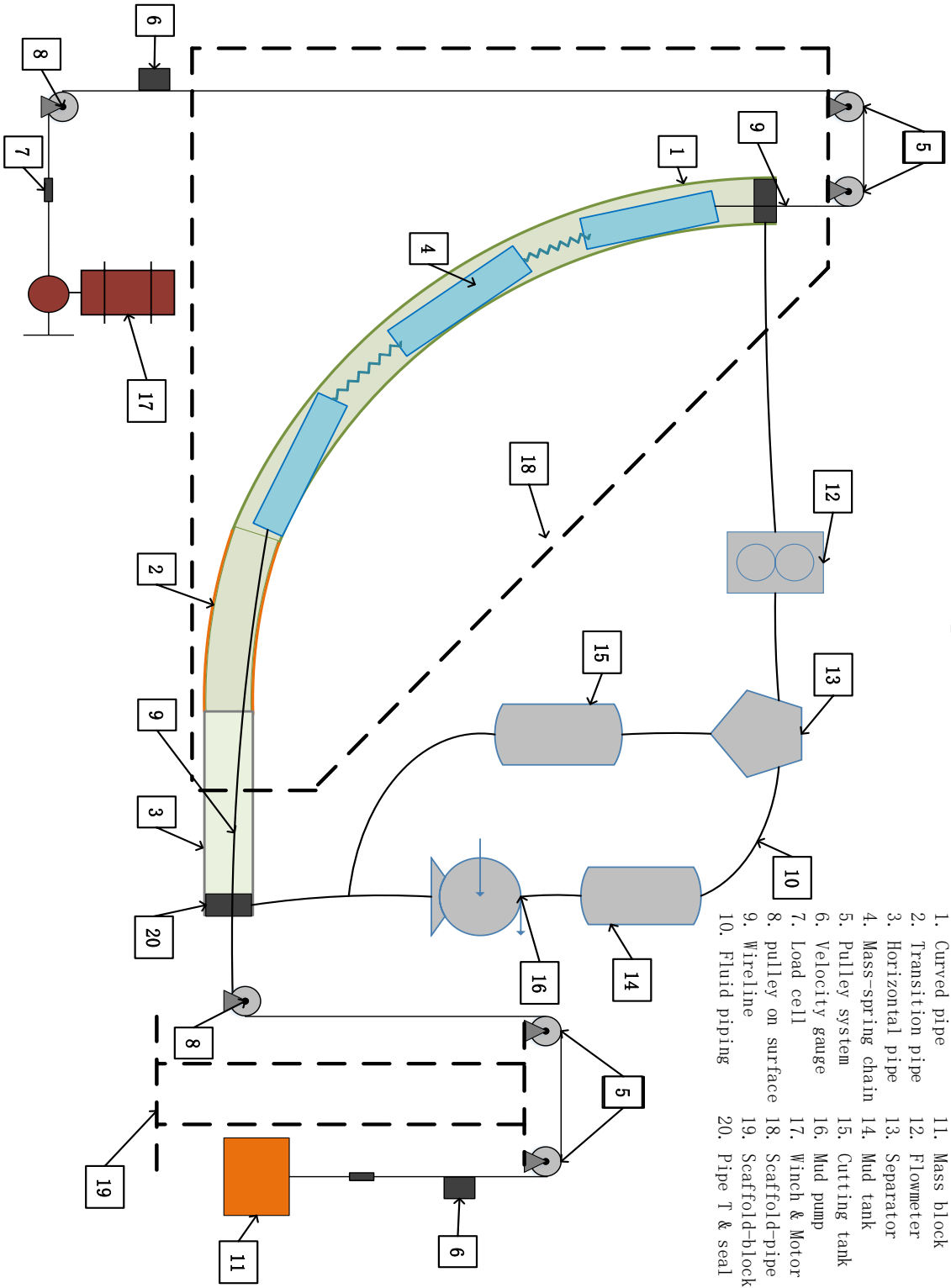
B. Flow chart to calculate static drag force

```
                    ╭─────────────────────────────╮
                    │ All necessary inputs to calculate static │
                    │ drag force such as survey data, drillstring │
                    │         information, etc.        │
                    ╰─────────────────────────────╯
                                   │
                                   ▼
                            ◇ Depend on normal force: ◇
                            ◇    positive or negative?  ◇
                   Positive                          Negative
                      │                                 │
                      ▼                                 ▼
        ┌────────────────────┐         ┌────────────────────┐
        │ Calculate normal force with │         │ Calculate normal force with │
        │   equation for positive    │         │   equation for negative    │
        │       normal force        │         │       normal force        │
        └────────────────────┘         └────────────────────┘
                      │                                 │
                      ▼                                 ▼
                   ◇ Choose the largest drag force as ◇
                   ◇      the correct drag force      ◇
                                   │
                            Largest drag force
                                   ▼
                    ╭─────────────────────────────╮
                    │   Finish calculation for this section   │
                    ╰─────────────────────────────╯
```

C. Programming (MATLAB code)

1. *Main program: Simulation*

```matlab
clear
clc
%% inputs
load('section.mat') % name of each section

%% tripping out parameters
%create simulated block position with specific average velocity and
%acceleration
v0 = 0; % m/s
a = 0.005; % m/s2
t0 = 10; %s
t1 = 13; %s
t2 = 30; %s
dt = 0.1; %s
[ BPOS, time, v_avg ] = simulated_BPOS( v0,a,t0,t1,t2,dt );

%% calculate static drag force
%load the input data, which is copied from excel and pre-processed in
the
%spreadsheet
%New static model to calculate drag force is applied in this
simulator.
%This model considers bend force when the drillpipe is attaching at
%the upper side of wellbore.
F_static = static_drag_force;

%% calculate displacement in each section
disp = displacement( F_static );

%% calculate length in each section
sec_lgth = section_length( disp );

%% calculate lower position of each section
pst_lwr = position_lower( sec_lgth );

%% define the input vector

%This function implements Runge-Kutta method. In this method, we
transfer
%the second order derivative to the first order derivative.

%such as:
%Section_end(1)=x(1)
%x(1)'=x(2)
%x(2)'=the detailed equation in odedisplacement.m

%Now we can define the input vector. The odd elements are the
%displacement. the even elements are first derivative of displacement,
```

```matlab
%i.e., velocity. In the static situation, the velocity is 0, so we use
0 as
%the initial value for the even elements.

xinitial=zeros(2*length(section),1);
for i=1:length(section)
    xinitial(i*2-1)=pst_lwr(i);
end

%% define a XX matrix to store all the position change during
simulation
XX(1,:)=pst_lwr; %at initial moment

%% define a HKL matrix to store all the HKL change during simulation
%define HKL. In our model, the HKL is the drag force at the upper
%end of drillstring, which is most close to the travelling block. It
equals
%to
n=length(section);
hkl(1)=F_static(n);

%% damping
load('dampen.mat') %Consider the damping

%% main simulation: dynamic simulation
%This is the main part of simulation. All equations are stored in
function
%odedisplacement.m.
%One thing must be noticed, the second order derivative of block
position
%is also an input which is the function of time. We have to update the
block
%acceleration i.e., the second order derivative before put equations
%into ode45 to calculate in a specific timespan. We use the
acceleration
%at the beginning of the time span as the representative in this
section.
%So we build a 'for' loop. for each time interval. We use the
acceleration
%and displacement as the input to calculate the displacement at the
end of
%each timespan, then the new timespan will be used as the input for
the
%next loop.

% load('BPOS.mat') %block position
% load('time.mat') %time record with BPOS
load('elasticity') % elasticity in each section, i.e. K in hook's law

for i=1:(length(BPOS)-1)
    i
    BPOS_current=BPOS(i);
```

```matlab
    timespan=[time(i) time(i+1)];
    [T,X]=ode45(@(t,x)
odedisplacement(t,x,BPOS_current,dampen,pst_lwr,disp),timespan,xinitia
l);
    xinitial=X(end,:);
    hkl(i+1)=elasticity(n)*((xinitial(2*n-1)+BPOS(i+1))-
(pst_lwr(n)+BPOS(1)-disp(n)));
    for j=1:n
        XX(i+1,j)=xinitial(2*j-1);
    end
end

%% draw the figure
draw_plot( hkl,time,XX,X,T,dampen,a,v_avg,t0,t2,dt,section )
%% warning
warning('It is done!')
```

2. *Function: displacement*

```matlab
function [ disp ] = displacement( F_static )

load('elasticity.mat') % elasticity in each section, i.e. K in hook's
law

disp = F_static./elasticity;


end
```

3. Function: odedisplacement

```matlab
function [ dx ] =
odedisplacement( t,x,BPOS_current,dampen,pst_lwr,disp)
%% some inputs
load('section.mat') % name of each section
load('ds.mat') % length of each section
load('incl.mat') % inclination at two ends, totally 7 points for 6
sections
load('incl_avg.mat') % average inclination for each section
load('incl_dlt.mat') % inclination change for each section
load('bf.mat') % calculated buoyance factor
load('ff.mat') % friction factor
load('g.mat') % gravity
load('w.mat') % unit weight for each section
load('elasticity.mat') % elasticity in each section, i.e. K in hook's
law
load('BPOS.mat') % block position

%% define the derivative vector
n = length(section);
dx = zeros(2*n,1);
%displacement
%t is the time
%dx is the first order derivative
%% with positive sign function
% dx(1)=x(2);
% dx(2)=1/(w(1)*ds(1))...
%      *(bf*w(1)*ds(1)*g*cos(incl_avg(1))+ff*sign(x(2))...
%      *abs(bf*w(1)*ds(1)*g*sin(incl_avg(1))...
%      -elasticity(1)*((x(1)-x(3))-(pst_lwr(1)-pst_lwr(2)-
disp(1)))*sin(incl_dlt(1)/2))...
%      -elasticity(1)*((x(1)-x(3))-(pst_lwr(1)-pst_lwr(2)-
disp(1)))*cos(incl_dlt(1)/2)...
%      -dampen*x(2));
% dx(3)=x(4);
% dx(4)=1/(w(2)*ds(2))...
%      *(bf*w(2)*ds(2)*g*cos(incl_avg(2))+ff*sign(x(4))...
%      *abs(bf*w(2)*ds(2)*g*sin(incl_avg(2))...
%      -elasticity(2)*((x(3)-x(5))-(pst_lwr(2)-pst_lwr(3)-
disp(2)))*sin(incl_dlt(2)/2)...
%      -elasticity(1)*((x(1)-x(3))-(pst_lwr(1)-pst_lwr(2)-
disp(1)))*sin(incl_dlt(2)/2))...
%      -elasticity(2)*((x(3)-x(5))-(pst_lwr(2)-pst_lwr(3)-
disp(2)))*cos(incl_dlt(2)/2)...
%      +elasticity(1)*((x(1)-x(3))-(pst_lwr(1)-pst_lwr(2)-
disp(1)))*cos(incl_dlt(2)/2)...
%      -dampen*x(4));
% dx(5)=x(6);
% dx(6)=1/(w(3)*ds(3))...
%      *(bf*w(3)*ds(3)*g*cos(incl_avg(3))+ff*sign(x(6))...
%      *abs(bf*w(3)*ds(3)*g*sin(incl_avg(3))...
```

```matlab
%       -elasticity(3)*((x(5)-x(7))-(pst_lwr(3)-pst_lwr(4)-
disp(3)))*sin(incl_dlt(3)/2)...
%       -elasticity(2)*((x(3)-x(5))-(pst_lwr(2)-pst_lwr(3)-
disp(2)))*sin(incl_dlt(3)/2))...
%       -elasticity(3)*((x(5)-x(7))-(pst_lwr(3)-pst_lwr(4)-
disp(3)))*cos(incl_dlt(3)/2)...
%       +elasticity(2)*((x(3)-x(5))-(pst_lwr(2)-pst_lwr(3)-
disp(2)))*cos(incl_dlt(3)/2)...
%       -dampen*x(6));
% dx(7)=x(8);
% dx(8)=1/(w(4)*ds(4))...
%       *(bf*w(4)*ds(4)*g*cos(incl_avg(4))+ff*sign(x(8))...
%       *abs(bf*w(4)*ds(4)*g*sin(incl_avg(4))...
%       -elasticity(4)*((x(7)+BPOS_current)-(pst_lwr(4)+BPOS(1)-
disp(4)))*sin(incl_dlt(4)/2)...
%       -elasticity(3)*((x(5)-x(7))-(pst_lwr(3)-pst_lwr(4)-
disp(3)))*sin(incl_dlt(4)/2))...
%       -elasticity(4)*((x(7)+BPOS_current)-(pst_lwr(4)+BPOS(1)-
disp(4)))*cos(incl_dlt(4)/2)...
%       +elasticity(3)*((x(5)-x(7))-(pst_lwr(3)-pst_lwr(4)-
disp(3)))*cos(incl_dlt(4)/2)...
%       -dampen*x(8));
%% with negative sign fuction, this should be the right one!!!
% dx(1)=x(2);
% dx(2)=1/(w(1)*ds(1))...
%       *(bf*w(1)*ds(1)*g*cos(incl_avg(1))-ff*sign(x(2))...
%       *abs(bf*w(1)*ds(1)*g*sin(incl_avg(1))...
%       -elasticity(1)*((x(1)-x(3))-(pst_lwr(1)-pst_lwr(2)-
disp(1)))*sin(incl_dlt(1)/2))...
%       -elasticity(1)*((x(1)-x(3))-(pst_lwr(1)-pst_lwr(2)-
disp(1)))*cos(incl_dlt(1)/2)...
%       -dampen*x(2));
% dx(3)=x(4);
% dx(4)=1/(w(2)*ds(2))...
%       *(bf*w(2)*ds(2)*g*cos(incl_avg(2))-ff*sign(x(4))...
%       *abs(bf*w(2)*ds(2)*g*sin(incl_avg(2))...
%       -elasticity(2)*((x(3)-x(5))-(pst_lwr(2)-pst_lwr(3)-
disp(2)))*sin(incl_dlt(2)/2)...
%       -elasticity(1)*((x(1)-x(3))-(pst_lwr(1)-pst_lwr(2)-
disp(1)))*sin(incl_dlt(2)/2))...
%       -elasticity(2)*((x(3)-x(5))-(pst_lwr(2)-pst_lwr(3)-
disp(2)))*cos(incl_dlt(2)/2)...
%       +elasticity(1)*((x(1)-x(3))-(pst_lwr(1)-pst_lwr(2)-
disp(1)))*cos(incl_dlt(2)/2)...
%       -dampen*x(4));
% dx(5)=x(6);
% dx(6)=1/(w(3)*ds(3))...
%       *(bf*w(3)*ds(3)*g*cos(incl_avg(3))-ff*sign(x(6))...
%       *abs(bf*w(3)*ds(3)*g*sin(incl_avg(3))...
%       -elasticity(3)*((x(5)-x(7))-(pst_lwr(3)-pst_lwr(4)-
disp(3)))*sin(incl_dlt(3)/2)...
```

```matlab
%      -elasticity(2)*((x(3)-x(5))-(pst_lwr(2)-pst_lwr(3)-
disp(2)))*sin(incl_dlt(3)/2))...
%      -elasticity(3)*((x(5)-x(7))-(pst_lwr(3)-pst_lwr(4)-
disp(3)))*cos(incl_dlt(3)/2)...
%      +elasticity(2)*((x(3)-x(5))-(pst_lwr(2)-pst_lwr(3)-
disp(2)))*cos(incl_dlt(3)/2)...
%      -dampen*x(6));
% dx(7)=x(8);
% dx(8)=1/(w(4)*ds(4))...
%      *(bf*w(4)*ds(4)*g*cos(incl_avg(4))-ff*sign(x(8))...
%      *abs(bf*w(4)*ds(4)*g*sin(incl_avg(4))...
%      -elasticity(4)*((x(7)+BPOS_current)-(pst_lwr(4)+BPOS(1)-
disp(4)))*sin(incl_dlt(4)/2)...
%      -elasticity(3)*((x(5)-x(7))-(pst_lwr(3)-pst_lwr(4)-
disp(3)))*sin(incl_dlt(4)/2))...
%      -elasticity(4)*((x(7)+BPOS_current)-(pst_lwr(4)+BPOS(1)-
disp(4)))*cos(incl_dlt(4)/2)...
%      +elasticity(3)*((x(5)-x(7))-(pst_lwr(3)-pst_lwr(4)-
disp(3)))*cos(incl_dlt(4)/2)...
%      -dampen*x(8));
%% without sign function, and the positive sign
dx(1)=x(2);
dx(2)=1/(w(1)*ds(1))...
    *(bf*w(1)*ds(1)*g*cos(incl_avg(1))+ff...
    *abs(bf*w(1)*ds(1)*g*sin(incl_avg(1))...
    -elasticity(1)*((x(1)-x(3))-(pst_lwr(1)-pst_lwr(2)-
disp(1)))*sin(incl_dlt(1)/2))...
    -elasticity(1)*((x(1)-x(3))-(pst_lwr(1)-pst_lwr(2)-
disp(1)))*cos(incl_dlt(1)/2)...
    -dampen*x(2));
dx(3)=x(4);
dx(4)=1/(w(2)*ds(2))...
    *(bf*w(2)*ds(2)*g*cos(incl_avg(2))+ff...
    *abs(bf*w(2)*ds(2)*g*sin(incl_avg(2))...
    -elasticity(2)*((x(3)-x(5))-(pst_lwr(2)-pst_lwr(3)-
disp(2)))*sin(incl_dlt(2)/2)...
    -elasticity(1)*((x(1)-x(3))-(pst_lwr(1)-pst_lwr(2)-
disp(1)))*sin(incl_dlt(2)/2))...
    -elasticity(2)*((x(3)-x(5))-(pst_lwr(2)-pst_lwr(3)-
disp(2)))*cos(incl_dlt(2)/2)...
    +elasticity(1)*((x(1)-x(3))-(pst_lwr(1)-pst_lwr(2)-
disp(1)))*cos(incl_dlt(2)/2)...
    -dampen*x(4));
dx(5)=x(6);
dx(6)=1/(w(3)*ds(3))...
    *(bf*w(3)*ds(3)*g*cos(incl_avg(3))+ff...
    *abs(bf*w(3)*ds(3)*g*sin(incl_avg(3))...
    -elasticity(3)*((x(5)-x(7))-(pst_lwr(3)-pst_lwr(4)-
disp(3)))*sin(incl_dlt(3)/2)...
    -elasticity(2)*((x(3)-x(5))-(pst_lwr(2)-pst_lwr(3)-
disp(2)))*sin(incl_dlt(3)/2))...
```

```matlab
        -elasticity(3)*((x(5)-x(7))-(pst_lwr(3)-pst_lwr(4)-
disp(3)))*cos(incl_dlt(3)/2)...
        +elasticity(2)*((x(3)-x(5))-(pst_lwr(2)-pst_lwr(3)-
disp(2)))*cos(incl_dlt(3)/2)...
        -dampen*x(6));
dx(7)=x(8);
dx(8)=1/(w(4)*ds(4))...
    *(bf*w(4)*ds(4)*g*cos(incl_avg(4))+ff...
    *abs(bf*w(4)*ds(4)*g*sin(incl_avg(4))...
    -elasticity(4)*((x(7)+BPOS_current)-(pst_lwr(4)+BPOS(1)-
disp(4)))*sin(incl_dlt(4)/2)...
    -elasticity(3)*((x(5)-x(7))-(pst_lwr(3)-pst_lwr(4)-
disp(3)))*sin(incl_dlt(4)/2))...
    -elasticity(4)*((x(7)+BPOS_current)-(pst_lwr(4)+BPOS(1)-
disp(4)))*cos(incl_dlt(4)/2)...
    +elasticity(3)*((x(5)-x(7))-(pst_lwr(3)-pst_lwr(4)-
disp(3)))*cos(incl_dlt(4)/2)...
    -dampen*x(8));
%% with negative tanh function
% dx(1)=x(2);
% dx(2)=1/(w(1)*ds(1))...
%     *(bf*w(1)*ds(1)*g*cos(incl_avg(1))-ff*tanh(10000*x(2))...
%     *abs(bf*w(1)*ds(1)*g*sin(incl_avg(1))...
%     -elasticity(1)*((x(1)-x(3))-(pst_lwr(1)-pst_lwr(2)-
disp(1)))*sin(incl_dlt(1)/2))...
%     -elasticity(1)*((x(1)-x(3))-(pst_lwr(1)-pst_lwr(2)-
disp(1)))*cos(incl_dlt(1)/2)...
%     -dampen*x(2));
% dx(3)=x(4);
% dx(4)=1/(w(2)*ds(2))...
%     *(bf*w(2)*ds(2)*g*cos(incl_avg(2))-ff*tanh(10000*x(4))...
%     *abs(bf*w(2)*ds(2)*g*sin(incl_avg(2))...
%     -elasticity(2)*((x(3)-x(5))-(pst_lwr(2)-pst_lwr(3)-
disp(2)))*sin(incl_dlt(2)/2)...
%     -elasticity(1)*((x(1)-x(3))-(pst_lwr(1)-pst_lwr(2)-
disp(1)))*sin(incl_dlt(2)/2))...
%     -elasticity(2)*((x(3)-x(5))-(pst_lwr(2)-pst_lwr(3)-
disp(2)))*cos(incl_dlt(2)/2)...
%     +elasticity(1)*((x(1)-x(3))-(pst_lwr(1)-pst_lwr(2)-
disp(1)))*cos(incl_dlt(2)/2)...
%     -dampen*x(4));
% dx(5)=x(6);
% dx(6)=1/(w(3)*ds(3))...
%     *(bf*w(3)*ds(3)*g*cos(incl_avg(3))-ff*tanh(10000*x(6))...
%     *abs(bf*w(3)*ds(3)*g*sin(incl_avg(3))...
%     -elasticity(3)*((x(5)-x(7))-(pst_lwr(3)-pst_lwr(4)-
disp(3)))*sin(incl_dlt(3)/2)...
%     -elasticity(2)*((x(3)-x(5))-(pst_lwr(2)-pst_lwr(3)-
disp(2)))*sin(incl_dlt(3)/2))...
%     -elasticity(3)*((x(5)-x(7))-(pst_lwr(3)-pst_lwr(4)-
disp(3)))*cos(incl_dlt(3)/2)...
```

```matlab
%        +elasticity(2)*((x(3)-x(5))-(pst_lwr(2)-pst_lwr(3)-
disp(2)))*cos(incl_dlt(3)/2)...
%        -dampen*x(6));
% dx(7)=x(8);
% dx(8)=1/(w(4)*ds(4))...
%        *(bf*w(4)*ds(4)*g*cos(incl_avg(4))-ff*tanh(10000*x(8))...
%        *abs(bf*w(4)*ds(4)*g*sin(incl_avg(4))...
%        -elasticity(4)*((x(7)+BPOS_current)-(pst_lwr(4)+BPOS(1)-
disp(4)))*sin(incl_dlt(4)/2)...
%        -elasticity(3)*((x(5)-x(7))-(pst_lwr(3)-pst_lwr(4)-
disp(3)))*sin(incl_dlt(4)/2))...
%        -elasticity(4)*((x(7)+BPOS_current)-(pst_lwr(4)+BPOS(1)-
disp(4)))*cos(incl_dlt(4)/2)...
%        +elasticity(3)*((x(5)-x(7))-(pst_lwr(3)-pst_lwr(4)-
disp(3)))*cos(incl_dlt(4)/2)...
%        -dampen*x(8));
end
```

4. Function: position_lower

```matlab
function [ pst_lwr ] = position_lower( sec_lgth )

sec_lgth = flip(sec_lgth);
sec_lgth = cumsum(sec_lgth);
pst_lwr = flip(sec_lgth);

% finally, we can calculate the cumulative length, i.e. the position of
% lower in each section.

% assume the upper point of drillstring is fixed, and the lower
% point is free, so the drillstring will elongate downward.

% For the top section, the length only counts its own displacement.

% For the lower section, the length only counts its own length
% and the length above this section.

% For the lowest section, the length equals to sum of the length in
% all sections.

end
```

5. Function: section_length

```matlab
function [ sec_lgth ] = section_length( disp )

load('sprg.mat') % length of each spring or wireline in mass-spring
chain
load('ds.mat') % length of each drillpipe, i.e. the mass in mass-
spring chain

sec_lgth = sprg + ds + disp;

%we add the spring length in each section, drillstring length (mass
%block) length in each section, and the displacement in each section
%together, then we obtain the total length in each section.
end
```

6. Function: simulated_BPOS

```matlab
function [ BPOS, time, v_avg ] = simulated_BPOS( v0,a,t0,t1,t2,dt )

%example simulated_BPOS( 0,0.0067,10,25,100,0.1 )

%This function can calculate a series of simulated BPOS and time.
%v0 is the initial velocity. In our research, initial velocity should
be
%zero.
%a is the acceleration, we assume the acceleration is a constant for
%convenience.
%From t0 to t1, the drillstring is still to make the simulator be
stable.
%t1 is the acceleration time. From t0 to t1, the drillstring is
experiencing
%acceleration state.
%t2 is the constant velocity time. From t1 to t2, the drillstring is
%tripped out with constant velocity.
%the time interval is also a constant. for example 0.1 sec.

T0 = (0:dt:(t0-dt))';
T1 = (0:dt:(t1-t0))';
T2 = (dt:dt:t2-t1)';

BPOS0 = zeros(length(T0),1);
BPOS1 = v0*T1+0.5*a*T1.^2;
BPOS2 = (v0+a*(t1-t0))*T2+BPOS1(end);

v_avg = a*(t1-t0);

time = (0:dt:t2)';
BPOS = [BPOS0;BPOS1;BPOS2];

plot(time,BPOS);

end
```

7. Function: static_drag_force

```matlab
function [ F ] = static_drag_force()
% 1. Use the modified mathematical model mentioned in semester
project.
% 2. Derive two expressions for calculate the drag force at the upper
point in each section
% 3. Calculate the results and choose the larger value as the drag
force.
% The reason why I choose the larger value as the drag force:
% During tripping out, friction is always opposite to drag force, so
the
%larger result indicates drag force and friction are opposite.

% load the input data, which is copied from excel and pre-processed
load('section.mat') % name of each section
load('ds.mat') % length of each section
load('incl.mat') % inclination at two ends, totally 7 points for 6
sections
load('incl_avg.mat') % average inclination for each section
load('incl_dlt.mat') % inclination change for each section
load('bf.mat') % calculated buoyance factor
load('ff.mat') % friction factor
load('g.mat') % gravity
load('w.mat') % unit weight for each section

% define unit weight manually
% w = Bf*7.22; % kg/m 2-3/8
% w = Bf*10.19; % kg/m 2-7/8
% w = Bf*14.14; % kg/m 3-1/2
% w = Bf*17.63; % kg/m 4
% w = Bf*20.46; % kg/m 4-5

%from the bottom, calculate the forces in each section at the static
state

% For the first component, there is no force at the lower end because
% the lower end is off the bottom.
% Therefore, the equation is a little bit different, so we solve it
first.
% Define matrix f is N by 2, N is the total number of sections in
system.
% For each section, two force will be calculated, then pick the bigger
one
% as the real drag force and stored in F, which is N by 1.
f = zeros(length(section),2); %store drag force for two scenarios
F = zeros(length(section),1); %store correct drag force
f(1,1) = bf*w(1)*ds(1)*g*(cos(incl_avg(1))+ff*sin(incl_avg(1)))/...
    (ff*sin(incl_dlt(1)/2)+cos(incl_dlt(1)/2));
f(1,2) = bf*w(1)*ds(1)*g*(cos(incl_avg(1))-ff*sin(incl_avg(1)))/...
    (-ff*sin(incl_dlt(1)/2)+cos(incl_dlt(1)/2));
F(1) = max(f(1,:));
```

```matlab
% for rest pipe, we have general equations which can be applied,
% and the procedure is the same as the first section.
for i = 2:length(section)
    for j = 1:2
        if j == 1
            f(i,j) =
(bf*w(i)*ds(i)*g*(cos(incl_avg(i))+ff*sin(incl_avg(i))))...
                -F(i-1)*(ff*sin(incl_dlt(i)/2)-
cos(incl_dlt(i)/2)))/...
                (ff*sin(incl_dlt(1)/2)+cos(incl_dlt(1)/2));
        elseif j == 2
            f(i,j) = (bf*w(i)*ds(i)*g*(cos(incl_avg(i))-
ff*sin(incl_avg(i)))...
                +F(i-
1)*(ff*sin(incl_dlt(i)/2)+cos(incl_dlt(i)/2)))/...
                (-ff*sin(incl_dlt(1)/2)+cos(incl_dlt(1)/2));
            F(i) = max(f(i,:));
        end
    end
end
% Horizontal section_drillpipe

%Calculate the normal force for each section based on the modified
%mathematical model in specialization project. For the negative normal
%force, it indicates that drillstring attaches at the upper side of
the
%wellbore. In buildup section, it is the side force.

N(1) = bf*w(1)*ds(1)*g*sin(incl_avg(1))-F(1)*sin(incl_dlt(1)/2);

for i = 2:length(section)
    N(i) = bf*w(i)*ds(i)*g*sin(incl_avg(i))-(F(i-
1)+F(i))*sin(incl_dlt(i)/2);
end

end
```

8. *Function: draw plot*

```matlab
function draw_plot( hkl,time,XX,X,T,dampen,a,v_avg,t0,t2,dt,section )
%This function will draw all the necessary figures about results.
n = size(XX,2);
%%
figure(1)

plot(time,hkl,'LineWidth',3)
title({['\fontsize{15}Simulated HKL vs. Time'];...
    ['\fontsize{10}Dampen: ',num2str(mean(dampen)),' N/(m/s)',...
    '  \fontsize{10} Acceleration: ',num2str(a),'
\fontsize{10}m/s2',...
    '  \fontsize{10} Average velocity: ',num2str(v_avg),' m/s']})

xlabel('Time (sec)','FontSize',14)
ylabel('Hook load (N)','FontSize',14)

grid on

xlim([t0-5,t2])

%%
figure(2)
for i=1:n
    subplot(ceil(n/ceil(sqrt(n))),ceil(sqrt(n)),i);
    plot(time,XX(:,i),'LineWidth',2)
    title({['\fontsize{15}Displacement of section:
',num2str(cell2mat(section(i)))];...
        ['\fontsize{10}Tripping out distance: ',num2str(1000*(XX(1,i)-
XX(end,i))),' mm']})
    xlabel('Time (sec)','FontSize',10)
    ylabel('MD (m)','FontSize',10)
    grid on
    set(gca,'YDir','reverse')
    xlim([t0-5,t2])
end

%%
figure(3)
for i=1:n
    subplot(ceil(n/ceil(sqrt(n))),ceil(sqrt(n)),i);
    plot(T,X(:,2*i-1),'LineWidth',2)
    title({['\fontsize{15}Disp at last ',num2str(dt),' s in section
',...
        num2str(cell2mat(section(i)))];...
        ['\fontsize{10}Tripping out distance: ',num2str(1000*(X(1,2*i-
1)-X(end,2*i-1))),' mm']})
    xlabel('Time (sec)','FontSize',10)
    ylabel('MD (m)','FontSize',10)
    grid on
    set(gca,'YDir','reverse')
```

```matlab
    xlim([T(1),T(end)])
end
%%
figure(4)
for i=1:n
    subplot(ceil(n/ceil(sqrt(n))),ceil(sqrt(n)),i);
    plot(T,X(:,2*i),'LineWidth',2)
    title({['\fontsize{15}Velocity at last ',num2str(dt),' s in
section ',...
        num2str(cell2mat(section(i)))];...
        ['\fontsize{10}Velocity: ',num2str(1000*(mean(X(:,2*i)))),'
mm/s']})
    xlabel('Time (sec)','FontSize',10)
    ylabel('Velocity (m/s)','FontSize',10)
    grid on
    set(gca,'YDir','reverse')
    xlim([T(1),T(end)])
end

end
```

Survey data - buildup section

WELLBORE_ID	Depth MD [m]	Incli deg	Azim deg	Depth TVD [m]	N/S [m]	E/W [m]	D-Leg	V Sect [m]	Delta Inclination	Delta MD	Delta TVD	Delta Horizontal	Horizontal	Lab MD [m]	Lab TVD [m]	Lab Hori [m]
NO 34/10-C-47	740.5	12.9	142.0	738.7	31.5	22.8	1.9	15.7	10.8	70.5	69.2	13.3	36.0	0.00	0.00	0.00
NO 34/10-C-47	777.0	15.7	141.7	774.1	24.4	28.3	2.3	22.6	14.3	36.5	35.4	9.0	45.0	0.55	0.53	0.13
NO 34/10-C-47	804.5	18.4	141.5	800.3	18.1	33.3	3.0	30.5	17.0	27.5	26.3	8.1	53.0	0.96	0.92	0.26
NO 34/10-C-47	832.2	20.8	141.2	826.4	10.8	39.1	2.6	39.7	19.6	27.7	26.1	9.3	62.3	1.37	1.31	0.39
NO 34/10-C-47	859.9	22.9	141.0	852.1	2.8	45.6	2.3	49.9	21.8	27.7	25.7	10.3	72.6	1.79	1.70	0.55
NO 34/10-C-47	886.5	25.1	140.5	876.4	-5.5	52.4	2.6	60.7	24.0	26.6	24.3	10.8	83.4	2.19	2.06	0.71
NO 34/10-C-47	914.4	26.9	140.3	901.6	-15.0	60.2	1.9	72.8	26.0	27.9	25.1	12.3	95.7	2.60	2.44	0.89
NO 34/10-C-47	941.5	29.4	138.8	925.8	-24.8	68.6	2.8	85.7	28.1	27.1	24.3	12.0	107.7	3.01	2.80	1.07
NO 34/10-C-47	969.5	31.6	137.2	949.6	-35.2	78.0	2.6	99.7	30.5	28.0	23.8	14.9	122.5	3.43	3.16	1.30
NO 34/10-C-47	996.7	34.7	136.8	972.3	-46.1	88.1	3.4	114.5	33.1	27.1	22.7	14.8	137.3	3.83	3.50	1.52
NO 34/10-C-47	1024.7	36.5	135.7	995.2	-57.8	99.4	2.0	130.8	35.6	28.1	22.8	16.3	153.7	4.25	3.84	1.76
NO 34/10-C-47	1052.2	35.1	136.1	1017.4	-69.4	110.6	1.5	146.9	35.8	27.5	22.3	16.1	169.7	4.67	4.17	2.00
NO 34/10-C-47	1079.8	35.2	136.1	1040.0	-80.8	121.6	0.1	162.3	35.1	27.6	22.5	15.9	185.6	5.08	4.51	2.24
NO 34/10-C-47	1106.2	35.8	135.0	1061.5	-91.6	132.6	0.7	178.2	35.5	26.5	21.6	15.4	201.0	5.47	4.83	2.47
NO 34/10-C-47	1133.7	37.9	135.6	1083.5	-103.3	144.2	2.3	194.6	36.8	27.5	22.0	16.5	217.4	5.89	5.16	2.72
NO 34/10-C-47	1161.4	39.7	136.2	1105.1	-115.7	156.2	2.0	212.0	38.8	27.6	21.6	17.3	234.8	6.30	5.49	2.98
NO 34/10-C-47	1189.0	42.0	137.3	1126.0	-128.9	168.6	2.7	230.0	40.8	27.6	20.9	18.1	252.8	6.71	5.80	3.25
NO 34/10-C-47	1215.4	45.3	137.6	1145.1	-142.3	180.9	3.7	248.2	43.7	26.4	19.1	18.2	271.0	7.11	6.08	3.52
NO 34/10-C-47	1243.8	47.3	138.8	1164.7	-157.6	194.6	2.3	268.7	46.3	28.4	19.7	20.5	291.6	7.53	6.38	3.83
NO 34/10-C-47	1271.3	49.7	137.7	1182.9	-173.2	208.1	2.8	289.3	48.5	27.5	18.2	20.6	312.2	7.95	6.65	4.13
NO 34/10-C-47	1298.5	52.1	139.3	1200.1	-189.0	222.1	3.0	310.4	50.9	27.2	17.1	21.1	333.3	8.35	6.91	4.45
NO 34/10-C-47	1326.1	54.9	139.1	1216.5	-205.8	236.6	3.0	332.5	53.5	27.6	16.4	22.2	355.5	8.77	7.15	4.78
NO 34/10-C-47	1353.6	57.8	137.3	1231.7	-222.9	251.9	3.6	355.5	56.4	27.5	15.3	22.9	378.4	9.18	7.38	5.13
NO 34/10-C-47	1381.2	58.9	136.9	1246.2	-240.1	267.9	1.2	378.9	58.3	27.6	14.5	23.5	401.9	9.59	7.60	5.48
NO 34/10-C-47	1408.5	60.9	135.1	1259.9	-257.0	284.3	2.9	402.5	59.9	27.3	13.7	23.6	425.5	10.00	7.80	5.83

DP data

OD		ID	Weight ppf		Crosssection
inch		inch	ppf	kg/m	mm2
2.375		1.995	4.85	7.22	842
2.875		2.441	6.85	10.19	1169
3.500		2.992	9.50	14.14	1671
4.000		3.478	11.85	17.63	1984
4.500		3.958	13.75	20.46	2322

On-site scale

OpenHole	
Measured length	668.0 m
Hole size	24.0 inch

Casing	
csg OD	20.0 inch
csg grade	N-80 grade
csg weight	133 ppf 198 kg/m
csg ID	18.73 inch

DP 6-5/8 in	
DP OD	6.625 inch
DP weight	29.41 ppf 43.8 kg/m
DP ID	5.965 inch

Tripping out	
distance	30 m
velocity	0.1 m/s

downscale factor	66.8
ppf->kg/m	1.488
ρ_steel	7800 kg/m3
Young's r	220000 Mpa

Lab scale

OpenHole	
Pipe len	10.0 m
Hole size	0.4 inch

Casing	
csg OD	0.30 inch
csg grad	N-80 grade
csg weig	0.0444 kg/m
csg ID	0.28 inch

DP 6-5/8 in	
DP OD	0.10 inch
DP weig	0.0098 kg/m
DP ID	0.09 inch

Tripping out	
distance	0.4491 m
velocity	0.0015 m/s

Casing	
csg OD	5.00 inch
csg grade	N-80 grade
csg weigl	17.1 kg/m
csg ID	4.78 inch

DP	2.375 inch
DP OD	2.375 inch
DP weigl	7.217 kg/m
DP ID	1.995 inch

DP	2.875 inch
DP OD	2.875 inch
DP weigl	10.193 kg/m
DP ID	2.441 inch

DP	3.5 inch
DP OD	3.500 inch
DP weigl	14.136 kg/m
DP ID	2.992 inch

DP	4 inch
DP OD	4.000 inch
DP weigl	17.633 kg/m

5.2 24" section

START: 28.11.2005 21:30 436 mMD
END : 22.12.2005 21:00 1508 mMD

A 20" casing N-80. 133 lbs/ft with Antares ER connections was installed in the 24" hole.

Size O.D. in.	Nominal Weight T & C lbs/ft	Grade	Collapse Resistance psi	Internal Yield Pressure at Minimum Yield, psi				Joint Strength 1000 lbs			Body Yield 1000 lbs	Wall in.	I.D. in.	Drift Diameter in.	
				PE	STC	LTC	BTC	STC	LTC	BTC				API	LSS
20.000	133.00	N-80	1600	4450	4450LR	4450LR	4450LR	1707	1976	2877	3091	0.635	18.730	18.542	

using 6-5/8'' DP in experiment

Original elastic force				Lab scale elastic force	
End	Force (N)			End	Force (N)
upper	544884		downscale->	upper	8157
lower	458562			lower	6865

The metal mass block suspended at lower end with **one fixed pulley**

700 kg

The result need to modified due to the model changed

Original weight of DP			Weight of DP in lab
16158 kg		downscale->	241.89 kg

5.53 m 6-5/8 in DP needed

33.52 m 2-3/8 in DP needed

If we keep using 6-5/8 drillstring in a lab scaling model, we still need very large elastic force at the lower end, i.e. a very big mass block. Perhaps we can use smaller drillpipe

using 2-3/8'' DP in experiment

Original elastic force				Lab scale elastic force	
End	Force (N)			End	Force (N)
upper	132340		downscale->	upper	1981
lower	92568			lower	1386
normal	-90265			normal	-1351

The metal mass block suspended at lower end with **one fixed pulley**

141 kg

Stiffness			Stiffness in Lab
277310 N/m		downscale->	4151 N/m

Original weight of DP in bended section			Weight of DP in lab
4821 kg		downscale->	72.17 kg

	2-3/8''	2-7/8''	3-1/2''	4''	4-1/2''
	10.0	7.1	5.1	4.1	3.5

using 2-7/8'' DP in experiment

Original elastic force with 2-7/8 inch pipe				Lab scale elastic force	
End	Force (N)			End	Force (N)
upper	186780		downscale->	upper	2796
lower	130646			lower	1956
normal	-127396			normal	-1907

The metal mass block suspended at lower end with **one fixed pulley**

200 kg

Stiffness			Stiffness in Lab
385006 N/m		downscale->	5764 N/m

Original weight of DP in bended section			Weight of DP in lab
6809 kg		downscale->	101.93 kg

	2-3/8''	2-7/8''	3-1/2''	4''	4-1/2''
	14.1	10.0	7.2	5.8	5.0

using 3-5'' DP in experiment

Original elastic force with 3-5 inch pipe				Lab scale elastic force	
End	Force (N)			End	Force (N)
upper	259182		downscale->	upper	3880
lower	181289			lower	2714
normal	-176780			normal	-2646

The metal mass block suspended at lower end with **one fixed pulley**

277 kg

Stiffness			Stiffness in Lab
550338 N/m		downscale->	8239 N/m

Original weight of DP in bended section			Weight of DP in lab
9443 kg		downscale->	141.36 kg

	2-3/8''	2-7/8''	3-1/2''	4''	4-1/2''
	19.6	13.9	10.0	8.0	6.9

Original elastic force with 4 inch pipe			Lab scale elastic force		
End	Force (N)		End	Force (N)	
upper	323153	downscale->	upper	4838	
lower	226035		lower	3384	
normal	-220412		normal	-3300	

The metal mass block suspended at lower end with **one fixed pulley**

345 kg

Stiffness			Stiffness in Lab		
653423 N/m		downscale->	9782 N/m		

Original weight of DP in bended section			Weight of DP in lab					
11779 kg		downscale->	176.33 kg	2-3/8''	2-7/8''	3-1/2''	4''	4-1/2''
				24.4	17.3	12.5	10.0	8.6

Original elastic force with 4-5 inch pipe			Lab scale elastic force		
End	Force (N)		End	Force (N)	
upper	375026	downscale->	upper	5614	
lower	262318		lower	3927	
normal	-255793		normal	-3829	

The metal mass block suspended at lower end with **one fixed pulley**

401 kg

Stiffness			Stiffness in Lab		
764742 N/m		downscale->	11448 N/m		

Original weight of DP in bended section			Weight of DP in lab					
13667 kg		downscale->	204.60 kg	2-3/8''	2-7/8''	3-1/2''	4''	4-1/2''
				28.4	20.1	14.5	11.6	10.0

E. Risk analysis of laboratory activities

		Prepared by	Number	Date
NTNU	Hazardous activity identification process	HSE section	HMSRV-26/01	09.01.2013
HSE ☐		Approved by	Replaces	
		The Rector		01.12.2006

Unit: *(Department)* Department of Petroleum Engineering and Applied Geophysics   **Date:** 15th , Oct, 2014

Line manager: Egil Tjåland, Head of Department

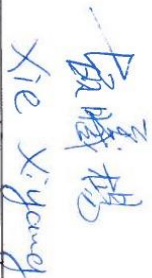**Participants in the identification process** (including their function):

Short description of the main activity/main process: Specialization project for student Xiyang Xie. Test acceleration of the drill string in the lab, in the field and theoretically.

Is the project work purely theoretical? (YES/NO): NO   *Answer "YES" implies that supervisor is assured that no activities requiring risk assessment are involved in the work. If YES, briefly describe the activities below. The risk assessment form need not be filled out.*

Signatures: *Responsible supervisor:*   Student:

ID nr.	Activity/process	Responsible person	Existing documentation	Existing safety measures	Laws, regulations etc.	Comment
7463 52	Test acceleration of the drill string in the lab	Xiyang Xie	Previous thesis using similar laboratory equipment as instruction	Protection equipment in laboratory.	The Laboratory and workshop Handbook, NTNU Norwegian Working Environment Act §2-3	Laboratory work
7463 52	Test acceleration of the drill string based on field data	Xiyang Xie				Theoretical work
7463 52	Modelling acceleration of the drill string theoretically	Xiyang Xie				Theoretical work

Risk assessment

Prepared by	Number	Date
HSE section	HMSRV2603E	04.02.2011
Approved by		Replaces
The Rector		01.12.2006

Unit: *(Department)*Department of Petroleum Engineering and Applied Geophysics   **Date:** 15th, Oct, 2014

Line manager: Egil Tjåland, Head of Department

Participants in the identification process (including their function):

Short description of the main activity/main process: Specialization project for student Xiyang Xie. Test acceleration of the drill string in the lab, in the field and theoretically.

Signatures: *Responsible supervisor:*   *Student:*

Activity from the identification process form	Potential undesirable incident/strain	Likelihood:	Consequence:			Risk Value (human)	Comments/status Suggested measures
		Likelihood (1-5)	Human (A-E)	Environment (A-E)	Economy/ material (A-E)		
Test acceleration of the drill string in the lab	Electric shock	2	D	A	B	2D	Protect human by isolation wear equipment
Test acceleration of the drill string in the lab	Hurt by tools	4	A	A	A	4A	Practice before using the tools

Likelihood, e.g.:
1. *Minimal*
2. *Low*
3. *Medium*
4. *High*
5. *Very high*

Consequence, e.g.:
A. *Safe*
B. *Relatively safe*
C. *Dangerous*
D. *Critical*
E. *Very critical*

Risk value (each one to be estimated separately):
Human = Likelihood x Human Consequence
Environmental = Likelihood x Environmental consequence
Financial/material = Likelihood x Consequence for Economy/materiel

Risk assessment

Potential undesirable incident/strain

Identify possible incidents and conditions that may lead to situations that pose a hazard to people, the environment and any materiel/equipment involved.

Criteria for the assessment of likelihood and consequence in relation to fieldwork

Each activity is assessed according to a worst-case scenario. Likelihood and consequence are to be assessed separately for each potential undesirable incident. Before starting on the quantification, the participants should agree what they understand by the assessment criteria:

Likelihood

Minimal 1	Low 2	Medium 3	High 4	Very high 5
Once every 50 years or less	Once every 10 years or less	Once a year or less	Once a month or less	Once a week

Consequence

Grading	Human	Environment	Financial/material
E Very critical	May produce fatality/ies	Very prolonged, non-reversible damage	Shutdown of work >1 year.
D Critical	Permanent injury, may produce serious serious health damage/sickness	Prolonged damage. Long recovery time.	Shutdown of work 0.5-1 year.
C Dangerous	Serious personal injury	Minor damage. Long recovery time	Shutdown of work < 1 month
B Relatively safe	Injury that requires medical treatment	Minor damage. Short recovery time	Shutdown of work < 1week
A Safe	Injury that requires first aid	Insignificant damage. Short recovery time	Shutdown of work < 1day

The unit makes its own decision as to whether opting to fill in or not consequences for economy/materiel, for example if the unit is going to use particularly valuable equipment. It is up to the individual unit to choose the assessment criteria for this column.

Risk = Likelihood x Consequence

Please calculate the risk value for "Human", "Environment" and, if chosen, "Economy/materiel", separately.

About the column "Comments/status, suggested preventative and corrective measures":

Measures can impact on both likelihood and consequences. Prioritise measures that can prevent the incident from occurring; in other words, likelihood-reducing measures are to be prioritised above greater emergency preparedness, i.e. consequence-reducing measures.

NTNU

HSE/KS

Risk matrix

prepared by	Number	Date
HSE Section	HMSRV2604	8 March 2010
approved by	Page	Replaces
Rector	4 of 4	9 February 2010

MATRIX FOR RISK ASSESSMENTS at NTNU

		LIKELIHOOD				
		Very low	Low	Medium	High	Very high
CONSEQUENCE	Extremely serious	E1	E2	E3	E4	E5
	Serious	D1	D2	D3	D4	D5
	Moderate	C1	C2	C3	C4	C5
	Minor	B1	B2	B3	B4	B5
	Not significant	A1	A2	A3	A4	A5

Principle for acceptance criteria. Explanation of the colours used in the risk matrix.

Colour		Description
Red		Unacceptable risk. Measures must be taken to reduce the risk.
Yellow		Assessment range. Measures must be considered.
Green		Acceptable risk Measures can be considered based on other considerations.

NTNU

Det skapende universitet